A Statistical Modelling Approach Evaluating Explosive Volcanism as a Trigger of Millennial-Scale Climate Change

JACK WILLIAM CAMPBELL

A Statistical Modelling Approach

Evaluating Explosive Volcanism as a Trigger of

Millennial-Scale Climate Change

Jack Campbell

A thesis presented for the degree of MSc by Research (Volcanology)

The University of Durham

Department of Earth Sciences

United Kingdom

2022

Table of Contents

Abstract

A Statistical Modelling Approach Evaluating Explosive Volcanism as a Trigger of Millennial-Scale Climate Change

Jack Campbell

Although millennial-scale climate change events are well documented across an array of globally distributed paleoclimate records, their driving mechanics remain ambiguous; a single coherent theory with concrete evidence providing a comprehensive explanation of the nature and origin of these phenomena remains elusive. Here a statistical model uses explosive volcanism as the sole trigger of millennial-scale climate change to reconstruct the NGRIP δ^{18}O ice core chronology over the last 100 ka BP. The model takes numerous steps to address the inferred undercount in the volcanic catalogue by using a weighted probability Monte Carlo simulation approach to generate statistically grounded 'missing' eruptions. The results make a compelling case for the consideration of explosive volcanism as a potential trigger of millennial-scale climate change. A model using known eruptions generated a modelled δ^{18}O time-series significantly correlated with the NGRIP δ^{18}O time-series ($R^2 = 0.678$, $p < 0.001$). Another model using both known eruptions and statistically generated 'missing' eruptions generated the strongest reproduction of the NGRIP δ^{18}O time-series ($R^2 = 0.681$, $p < 0.001$), strongly supporting the hypothesis that unknown eruptions could have triggered millennial-scale climate change events that occurred during gaps in the known eruptions catalogue. The results also suggest it is highly likely that the abrupt climate transitions at the onset of the Younger Dryas and GS-20 had volcanic origins, using the recently dated rare supereruption doublet at the onset of GS-20 to underscore the importance of accurately dating eruptions to fully understand the potential climatic impacts of explosive volcanism. Future investigations should focus modelling attempts on shorter windows to adequately investigate the plausibility of explosive volcanism as a trigger of millennial-scale climate change at an individual event level while considering eruption dating uncertainties to address offset issues and maximise correlations between modelled and NGRIP δ^{18}O time-series.

List of Abbreviations

Abbreviation	Definition	Page
DO	Dansgaard-Oeschger	9
GS	Greenland Stadial	9
GI	Greenland Interstadial	9
AMOC	Atlantic Meridional Overturning Circulation	11
NH	Northern Hemisphere	11
SH	Southern Hemisphere	11
FWPH	Fresh Water Pulse Hypothesis	11
BA	Bølling-Allerød	12
YD	Younger Dryas	12
YDIH	Younger Dryas Impact Hypothesis	13
ITCZ	Intertropical Convergence Zone	18
VOLGRIPA	Volcano Global Risk Identification and Analysis Project	21
LaMEVE	Large Magnitude Explosive Volcanic Eruptions	21
NGRIP	North Greenland Ice Core Project	21
GRR	Gradual Recovery Rate	28
POI	Period of Interest	39
LSE	Laacher See Eruption	47
YTT	Youngest Toba Tuff	50

List of Model Variants

Model Name	Details
Model 1 ('Known Eruptions')	A theoretical model which used only known eruptions from the LaMEVE database over the last 100 ka BP with medium to high dating quality which satisfied magnitude threshold constraints (SH > M5, NH > M6).
Model 2 ('Uniform')	An experimental model which used a uniform distribution of random probability to assign a net volcanic forcing in each year. Eruptions filtered to meet magnitude threshold constraints (SH > M5, NH > M6). An M8 and M1 eruption had the same chance of occurring throughout.
Model 3 ('Weighted Probability')	A theoretical model which used a weighted probability calculation to generate random annual net volcanic forcing values. Calculations based on return periods from Rougier et al. (2018) and LaMEVE hemispheric distribution split (0.875(NH):0.125(SH)). An M1 eruption was much more likely to occur than an M8 eruption. Eruptions filtered to meet magnitude threshold constraints (SH > M5, NH > M6).
Model 4 ('Combination')	A theoretical model which used eruptions from Model 1 ('Known Eruptions') and filled in unknown years using the same approach as Model 3 ('Weighted Probability'). Eruptions filtered to meet magnitude threshold constraints (SH > M5, NH > M6). This model had the most accurate estimation of annual net volcanism (known eruptions plus an estimate for probable 'missing eruptions').

Acknowledgements

I would like to take this opportunity to say a huge thanks to my supervisor Prof. James Baldini for his invaluable guidance throughout this thesis; from the onset, he offered unwavering support and answered innumerable questions, no matter how small or inane. Without his expert knowledge and inspiring teaching, this thesis would not have been possible. Due to the pandemic, we never got the chance to meet in person, but this did not stop me from learning lifelong skills which I hope to use in future studies toward a PhD.

I would also like to take this opportunity to thank my friends and family who have always supported me in my studies. A special thanks to those who helped me blow off steam with much-needed pints and to those who had to endure my ramblings when I used them as a human mind map to think aloud and order my thoughts. Finally, I would like to thank everyone I met from the Earth Science department (most likely on zoom) for offering valuable insights and pointers for my thesis.

Dedication

I dedicate this work to my Nana in celebration of her 80th birthday. Her unconditional love, support and counsel have undoubtedly helped me get to this point, meaning this work is as much hers as it is mine. I hope she enjoys it. Happy Birthday, Nana!

Statement of Copyright

Section 1: Introduction

1.1: Literature Review

Abrupt climate change refers to significant alterations to climate, such as average temperature, over decades to centuries (National Research Council, 2001; Bengston et al., 2020). Geologic records show that considerable and expansive abrupt climate change occurred many times throughout Earth's history (Alley et al., 2003); perhaps the best-known examples of abrupt climate change occurred during the last glacial period (11.7 – 115 ka BP) in the form of Dansgaard-Oeschger (DO) events (Cimatoribus et al., 2013; Boers, 2018; Li and Born, 2019; Gottwald, 2021). Dansgaard-Oeschger events, first described by Dansgaard (1985), manifest in Greenland ice core $\delta^{18}O$ records over millennial time scales as sudden transitions from cold baseline Greenland Stadial (GS) conditions to warmer Greenland Interstadial (GI) conditions (Rasmussen et al., 2014; Boers, 2018; Lohmann and Ditlevsen, 2018). Based on relationships between $\delta^{18}O$ and temperature, abrupt warming between 10-15 °C occurs within decades (Lohmann and Ditlevsen, 2018), followed by a gentle return to baseline GS conditions within centennial to millennial timespans (Boers, 2018) (Figure 1).

DO events are well documented across an array of globally distributed records (Genty et al., 2003; Petersen et al., 2013; Lohmann et al., 2021), resulting in broad agreement regarding their duration and structure. However, the forcing mechanisms driving these events are not understood and remain widely debated (Schulz, 2002; Boers, 2018; Dima et al., 2018; Li and Born, 2019; Gottwald, 2021); the enigmatic nature of these phenomena means research surrounding their origin has become a cornerstone of paleoclimatology

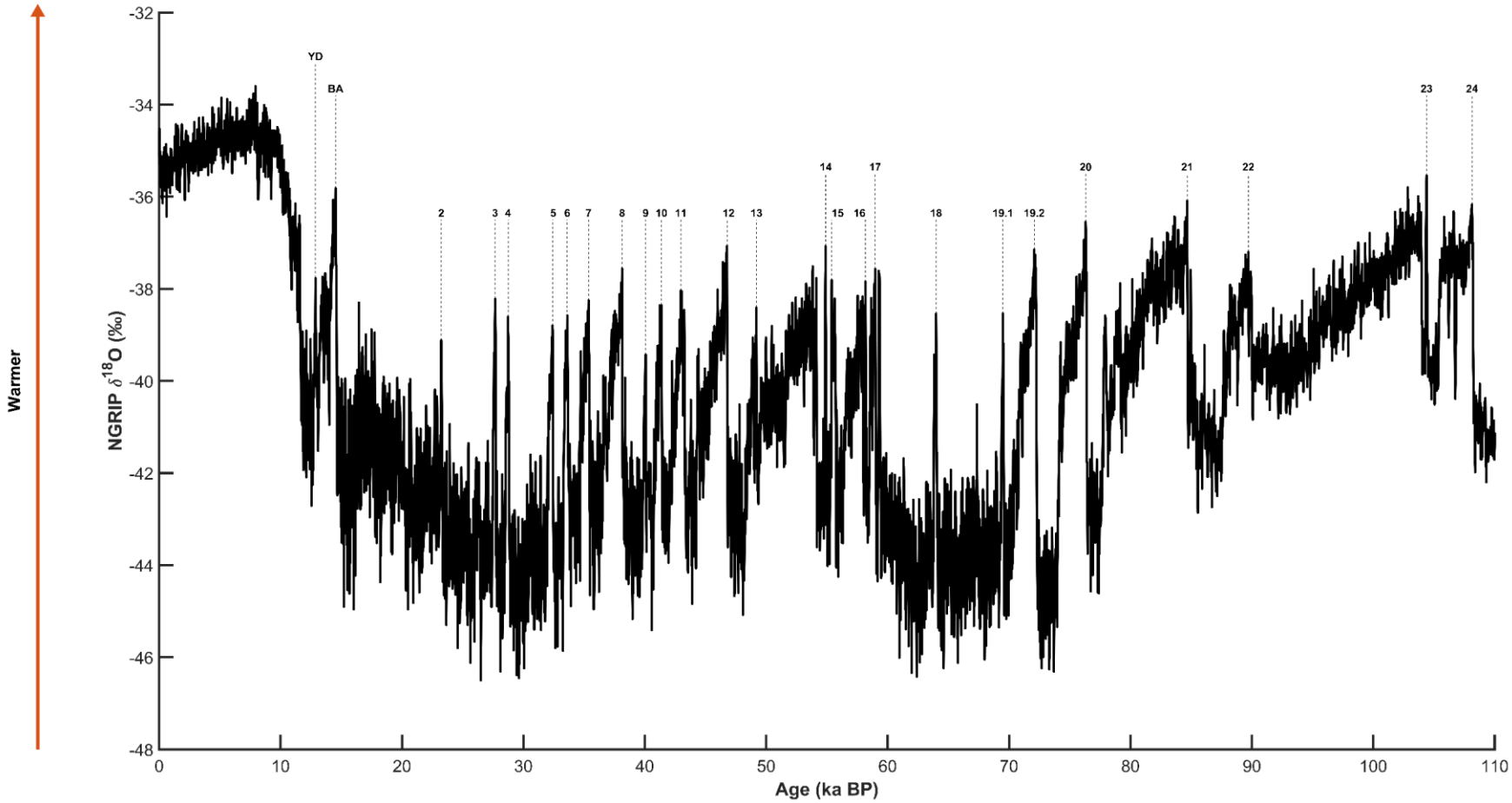

Figure 1: 24 classical DO events between 0-110 ka BP in terms of δ^{18}O (‰) from the NGRIP ice core chronology, including the Younger Dryas (YD) cold event (GS-1) and the Bølling–Allerød (BA) warm event (DO 1). Figure adapted from Schulz (2002).

(Ganopolski and Rahmstorf, 2002; Denton et al., 2005; Braun and Kurths, 2010). Debate within the researching community exists as a result of the vast number of contrasting theories proposing explanations for the nature of DO events (Schulz, 2002; Gottwald, 2021); developed theories range from prototype models to detailed computer simulations of coupled ocean-atmosphere general circulation models (Cimatoribus et al., 2013; Gottwald, 2021), each with different controlling features on DO events ranging from external forcing triggers to cyclical calving of the Greenland ice sheet (Schulz, 2002). However, some theories have gained more traction than others, with theories built on the premise that the ocean is the primary agent controlling DO events receiving the most research attention (Gottwald, 2021).

The Freshwater Pulse Hypothesis (FWPH) is the most widely accepted theory to explain DO events (Gottschalk et al., 2015). It argues that the delivery of a freshwater pulse to the North Atlantic perturbs and triggers large scale reorganisation of the Atlantic Meridional Overturning Circulation (AMOC) and cross-equatorial heat delivery (Guillevic et al., 2013; Gottschalk et al., 2015) because of altered salinity levels in top-waters (Bond et al., 1993). The FWPH relies on the link between the strengthening (weakening) of the AMOC and the delivery of warm equatorial water at an enhanced (decreased) rate, leading to warming (cooling) in the NH (SH) (Li and Born, 2019; Oka et al., 2021). The FWPH is popular due to the theory offering a possible explanation for the ‘bipolar seesaw’ documented in Antarctic and Greenland ice cores (Stocker and Johnsen, 2003; Oka et al., 2021), whereby the temperature expression of DO events in Greenland ice cores are broadly equal and opposite

to temperature expressions in Antarctic ice cores (Baldini et al., 2015; Li and Born, 2019; Oka et al., 2021).

However, there are many unresolved issues with the fundamental assumptions made by the FWPH. Using the Bølling–Allerød (BA) – Younger Dryas (YD) transition as an example, there is no physical evidence identifying a clear source path of the theorised triggering freshwater pulse from Lake Agassiz (Broecker, 2006; Carlson, 2010). Some theories propose a different source of freshwater, such as the Fennoscandian ice sheet (Dokken et al., 2013; Muschitiello et al., 2015), or an alternative flow path, such as drainage by the Mackenzie River into the Arctic Ocean rather than into the North Atlantic Ocean by the St. Lawrence River (Murton et al., 2010; Condron and Winsor, 2012; Not and Hillaire-Marcel, 2012). The lack of certainty in the source and drainage path of the freshwater pulse that supposedly triggered the BA-YD transition highlights the current lack of coherence and consistency of the FWPH, showing it is not a definitive theory explaining DO event occurrence.

Furthermore, the pivotal role of the overturning circulation in the FWPH is also disputed (Petersen et al., 2013; Gottschalk et al., 2015; Dima et al., 2018; Gottwald, 2021), and many modelling attempts using AMOC alterations to reconstruct DO events have proven problematic. For example, actual data reveals that freshwater pulses tend to come after abrupt climate transitions, which is a problem for many models which use these pulses to trigger the onset of DO events (Li and Born, 2019). Moreover, other modelling attempts have shown that the amount of warming caused by alterations in the AMOC alone is insufficient at replicating the magnitude of warming during DO events seen in ice core data

(Petersen et al., 2013). Finally, the assumption that DO event triggers always occur in the NH is a considerable issue with the FWPH. Recent proxy data reveals both leads and lags between DO event expression in Greenland and Antarctica (Dima et al., 2018); instances of DO event expression in Antarctica before Greenland highlights the possibility that DO event triggers are sometimes situated in the SH (Dima et al., 2018). These issues illustrate critical flaws in the fundamental assumptions made in the FWPH; this theory cannot account for all features of DO event nature.

The shortcomings of the FWPH encouraged the development of alternative theories, which propose different mechanisms to explain DO events. For example, one theory suggests that the periodic breaking and regeneration of a thick ice shelf east of Greenland controlled DO event duration by modulating the recovery rate from GI conditions back to baseline GS conditions (Petersen et al., 2013; Boers et al., 2018). Focussing on the most recent DO event, the Younger Dryas Impact Hypothesis (FWPH) suggests that an extra-terrestrial meteor impact potentially triggered the abrupt climate transition (Firestone et al., 2007; Israde-Alcántara et al., 2012; Holliday et al., 2014). However, this is a case-specific explanation for a period which is not statistically different from any other DO event (Nye and Condron, 2021); therefore, the YDIH is not an explanation that can extend to most other events.

To summarise, even though the FWPH is currently the dominant theory used to explain DO events, it cannot account for key features of DO event nature or accurately reconstruct DO events. In addition to this, the debate surrounding the application of the FWPH to the BA-YD transition, alongside the presence of alternative hypotheses suggesting contrasting

forcing mechanisms, illustrates the ongoing discourse surrounding DO events; a single coherent theory with concrete evidence providing a comprehensive explanation of the nature and origin of these phenomena remains elusive (Li and Born, 2019).

As the debate surrounding DO event nature remains unresolved, it is important to continue exploring how alternative mechanisms could potentially trigger DO events; explosive volcanism offers a possible and tenable alternative potential DO event trigger. Strong historical documentation of the significant natural forcing of explosive volcanic eruptions on abrupt climate change means no other natural forcing on climate is better understood over the last few hundred years (Minnis et al., 1993; Robock, 2000; Cole-Dai, 2010; Timmreck, 2012). For example, detailed instrumental monitoring measured a 0.5˚C global average cooling spanning two years after the eruption of Mount Pinatubo (1991), revealing important empirical evidence that explosive volcanism can trigger abrupt climate change (Hansen et al., 1992; Oppenheimer, 2011; Stenchikov et al., 1998). Furthermore, anecdotal and proxy evidence shows strong links between the eruption of Mount Tambora (1815 C.E.) and the widely reported 'year with no summer' in 1816 C.E. (Oppenheimer, 2011; Kandlbauer et al., 2013); for two years post-eruption, there was an estimated 5-6 Wm^{-2} reduction in radiative forcing (Brázdil et al., 2016; Brönnimann and Krämer, 2016). These eruptions are among the best-known examples of volcanism triggering abrupt climate change, albeit on timescales shorter than those associated with DO events. Furthermore, the Mount Pinatubo (1991 C.E.) eruption offers an exciting insight into future research on the link between volcanism and abrupt climate change through direct climate monitoring during explosive volcanic eruptions.

Historically, paleoclimatologists have disregarded a causal link between explosive volcanism and DO events because of the popularity of the FWPH and the high dating uncertainties of both climate and volcanological records (Baldini et al., 2018). The disregarding of the potential causal link persists due to the considerable chronological undercounts in the known volcanic catalogue, which is especially severe for eruptions large enough to trigger DO events (Furlan, 2010; Brown et al., 2014; Baldini et al., 2015; Kiyosugi et al., 2015; Cooper et al., 2018; Papale, 2018; Rougier et al., 2018; Lohmann and Svensson, 2020). Consequently, dating uncertainties and chronological gaps have prevented in-depth exploration of the link between explosive volcanism by compounding efforts to confidently attribute single DO events to large individual eruptions (Baldini et al., 2018; Lohmann and Svensson, 2020).

However, previous investigations that explored the link between DO events and explosive volcanism have found some critical breakthroughs. The finding that the DO event sequence is consistent with a random stationary process is especially notable (Lohmann and Ditlevsen, 2018), as this aligns perfectly with the nature of volcanic activity (Rougier et al., 2018). Furthermore, bipolar volcanic eruptions dated just before the onset of DO events occurred more frequently than by chance, with considerable confidence (>99%) (Lohmann and Svensson, 2020). Similarly, all known and radiometrically-dated large NH eruptions between 30-80 ka BP show association with abrupt Greenland cooling (>95% confidence) (Baldini et al., 2015). In contrast, the timing of SH explosive volcanism (known and unknown) correlates with the onset of DO events (>99% confidence) (Bay et al., 2004; Baldini et al., 2015). Furthermore, some well-dated eruptions strongly suggest that

explosive volcanism could potentially trigger DO events. For example, a recently documented volcanogenic sulphur spike associated with the Laacher See eruption at 12.880 ±0.040 ka BP represents a potential plausible trigger of the BA-YD transition (Baldini et al., 2018; Sun et al., 2020). Finally, volcanically triggered abrupt climate change potentially occurred during the Holocene, as revealed by the attribution of the onset of the Little Ice Age (1500 – 1900 A.D.) to explosive volcanism (Miller et al., 2012); consequently, it is crucial to acknowledge the potential present-day threat of volcanically triggered abrupt climate change.

Although recent studies have considerably progressed the understanding of the potential link between the timing of explosive volcanism and DO events, there has yet to be a focused effort to quantify a possible causative mechanism. Therefore, this study aims to investigate the feasibility of explosive volcanism as a trigger of abrupt millennial-scale climate change by modelling the potential impacts of explosive eruptions on abrupt climate changes over the last 100 ka BP. A better understanding of millennial-scale climate change is paramount for detecting and forecasting climate system alterations driven by anthropogenic activity (Blunier and Brook, 2001; Bard, 2002; Schulz, 2002; Riechers and Boers, 2021). These periods of abrupt climate change have widespread impacts globally and have often been the dominant expression of past paleoclimate variability (Alley et al., 1999; Keigwin, 1999; Li and Born, 2019), which is concerning considering the lack of acknowledgement of the potential rapidity of climate change currently shown by climate change policymakers (Alley et al., 2003; IPCC, 2021). With the Holocene revealing lower magnitude features of millennial-scale climate change, it is dangerous to assume these events will not occur in

the future (Schulz, 2002). With the events manifesting on human timescales, a modern contextualisation and consideration of these events is crucial (Baldini et al., 2015) because a similar warming occurring today superimposed on anthropogenic greenhouse gas warming could destabilise the Greenland ice sheet.

1.2: Understanding the Forcing Mechanisms of Explosive Volcanism on Abrupt Climate Change

Understanding how explosive volcanic eruptions force abrupt temperature changes over long timescales is crucial to model their potential impact over the last 100 ka BP successfully. The primary control of the direct climate change caused by explosive volcanism is the volume of sulphur-containing gases (such as sulphur dioxide and hydrogen sulphide) ejected into the stratosphere (Ramaswamy et al., 2006; Cole-Dai, 2010; Timmreck, 2012; Swingedouw et al., 2017). In the stratosphere, sulphur-containing particulates oxidise to form sulphuric acid vapours, which condense with water to form sulphate aerosols with a residence time between 1–3 years (Stenchikov et al., 1998; Robock, 2000; Ramaswamy et al., 2006; Timmreck, 2012; Pausata et al., 2015; Aubry et al., 2021). Stratospheric sulphate aerosols advect rapidly around the globe, directly altering the global radiation balance and energy budget (Stenchikov et al., 1998; Cole-Dai, 2010; Timmreck, 2012; Baldini et al., 2018); an increase in sulphate aerosol concentration in the stratosphere enhances the scattering of incoming shortwave radiation and increases the albedo of the stratosphere, resulting in net average global cooling (Stenchikov et al., 1998; Robock, 2000; Lechleitner et al., 2017; Aubry et al., 2021). For example, during the eruption of Mount Pinatubo (1991), radiative forcing mechanisms caused global average diffuse

sunlight to increase by 20% and total sunlight to decrease by 2.5% (Proctor et al., 2018). The understanding of how explosive volcanic eruptions alter the global energy budget is one of the most developed and best understood mechanisms of natural forcing on climate change (Cole-Dai, 2010) since its formulation after the eruption of Krakatoa (1883) (Schalter et al., 2009).

However, a currently poorly constrained but possible commonplace sustained volcanic influence on global climate up to several hundred years after an eruption may exist, suggesting that the impact of explosive volcanism on abrupt climate change is more complex than simply 1–3-year cooling caused by altering the net radiative forcing budget (Schalter et al., 2009; Baldini et al., 2015). The initial sulphate aerosol cooling may trigger long-term atmospheric reorganisation by forming a hemispheric temperature asymmetry, perturbing global atmospheric circulation patterns (Baldini et al., 2015; Lechleitner et al., 2017; Pausata et al., 2015). After an explosive NH eruption, the NH initially cools to a greater degree than the SH due to amplified aerosol scattering of insolation, increasing the temperature gradient across the hemispheres (Baldini et al., 2015; Lechleitner et al., 2017). Consequently, the Intertropical Convergence Zone (ITCZ) displaces southwards as it migrates towards the warmer hemisphere (Baldini et al., 2015; Muschitiello et al., 2015; Ridley et al., 2015; Colose et al., 2016; Lechleitner et al., 2017; Pausata et al., 2020). This displacement potentially compresses the Hadley and Ferrel cells in the SH, driving the SH Polar front south, warming northern regions of the Antarctic (Baldini et al., 2015). During periods of low greenhouse gas concentrations and low levels of insolation, such as the last glacial period, an explosive NH eruption may have initiated a cooling positive feedback loop

in the NH, resulting in Greenland cooling as well as Antarctic warming (Baldini et al., 2015). With these boundary conditions, sulphate aerosols injected into the NH stratosphere after a large NH explosive eruption would cause a more rapid and drastic initial cooling of the NH atmosphere compared to periods with higher insolation and greenhouse gas concentrations. The drastic cooling would facilitate NH glacier expansion consequent to NH sea ice expansion, causing a combined increase in the NH albedo effect. As a result, the AMOC would weaken, reducing the rate of warm water delivery from the equator to the NH, resulting in further NH cooling. The low levels of insolation and greenhouse gas concentrations would perpetuate this cycle, as low levels of NH heat accumulation could not counteract the cooling mechanisms triggered by the initial NH explosive volcanic eruption (Baldini et al., 2015) (Figure 2). Halting the positive feedback would rely on increased solar activity, greenhouse gas concentrations, or a larger explosive volcanic eruption in the SH to outweigh cooling mechanisms in the NH. During periods with similar boundary conditions, SH eruptions cause equal but opposite impacts compared to NH eruptions: the ITCZ shifts northwards because of a reversed hemispheric temperature gradient, compression of Hadley and Ferrel cells causes the northward displacement of the NH Polar front, resulting in DO event like warming periods in Greenland and cooling in Antarctica (Baldini et al., 2015; Ridley et al., 2015; Colose et al., 2016; Pausata et al., 2020).

It is crucial to acknowledge these dynamic impacts to understand the overall effect of explosive volcanism on climate. The assumption that all eruptions lead to only global uniform average cooling is overly simplistic (Baldini et al., 2015); focussing solely on global radiative forcing impacts of explosive volcanic eruptions underestimates the importance of

large high latitude eruptions (Baldini et al., 2015; Pausata et al., 2015). Furthermore, a consideration of the dynamic impacts of explosive volcanism is vital to plausibly link volcanism and the bipolar seesaw (Stenni et al., 2011; Baldini et al., 2015), as radiative forcing mechanics cannot account for warming after an explosive volcanic eruption beyond the lifetime of atmospheric aerosols; therefore, a tenable relationship between explosive volcanism and millennial-scale climate change only exists when considering the impacts of explosive volcanism on global atmospheric circulation (Baldini et al., 2015).

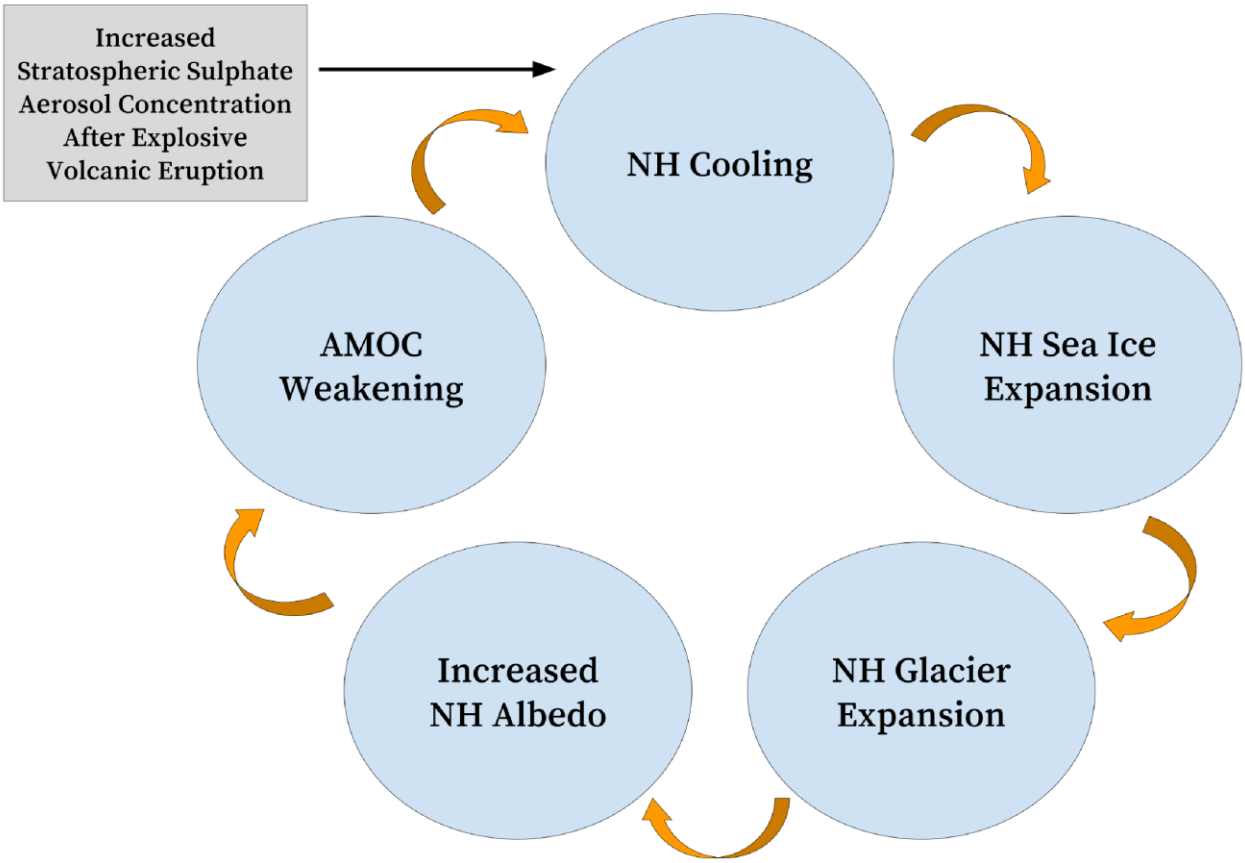

Figure 2: NH cooling positive feedback loop that occurred during the last glacial period, initiated by the increased stratospheric sulphate aerosol concentration after an explosive NH eruption. Visualised from Baldini et al. (2015).

Section 2: Methods

2.1: Intricacies of the Statistical Model

The model used to investigate the link between explosive volcanic eruptions and millennial-scale climate change utilised the following data: NGRIP δ^{18}O (‰) (North Greenland Ice Core Project members, 2004), Atmospheric CO_2 concentration (ppm) (Bereiter et al., 2015), global sea level (m) (Spratt and Lisiecki, 2016), and the VOLGRIPA (Volcano Global Risk Identification and Analysis Project) LaMEVE (Large Magnitude Explosive Volcanic Eruptions) database *(M)* (Crosweller et al., 2012; Brown et al., 2014) (Table 1). Calculating z-scores (a linear transformation calculating the difference between an individual data point and the dataset mean, expressing this in terms of standard deviations) for the paleoclimate datasets and transferring each dataset to years BP with annual resolution facilitated data handling and cross-correlation. The model used one of five equations to calculate annual Greenland δ^{18}O z-score values for each time slice; each equation is either an abrupt change equation (Eq. 1 and Eq.2), the baseline equation (Eq. 3) or a gradual recovery equation (Eq.4 and Eq.5), which take the form

$$\text{Eq. 1: } X_t = X_{t+1} + (n_t . u_t),$$

$$\text{Eq. 2: } X_t = X_{t+1} - (n_t . u_t),$$

$$\text{Eq. 3: } X_t = B_t,$$

$$\text{Eq. 4: } X_t = X_{t+1} - R_t,$$

$$\text{Eq. 5: } X_t = X_{t+1} + R_t,$$

where X is the modelled $\delta^{18}O$ value, t is the year of calculation (a BP), n is the climate sensitivity, B is the temperature baseline, R is the gradual recovery rate (yr^{-1}), and u is the magnitude constant. The pathway taken through the decision-tree algorithm determined the equation used in each year (Figure 3). The subsequent subsections explain the variables in each equation. The final output was a modelled Greenland temperature proxy record over the last 100 ka BP in the form of an annual resolution modelled Greenland $\delta^{18}O$ time-series (Rozanski et al., 1992).

Table 1: Details of the four key datasets used to calculate the modelled Greenland $\delta^{18}O$ time-series.

Dataset	Units	Details	Source
$\delta^{18}O$	per mille (‰)	• GICC05modelext chronology • -30 – 122210 a BP	North Greenland Ice Core Project members (2004)
CO_2	parts per million (ppm)	• AICC2012 chronology • 0 - 800 ka BP	Bereiter et al. (2015)
Sea Level	meters above present day (m)	• Annual chronology • 0 - 798 ka BP • Stacked based on 7 independent records	Spratt and Lisiecki (2016)

Dataset	Units	Details	Source
LaMEVE Catalogue	Magnitude *(M)*	• All known explosive volcanic eruptions over the Quaternary	Crosweller et al. (2012) Brown et al. (2014)

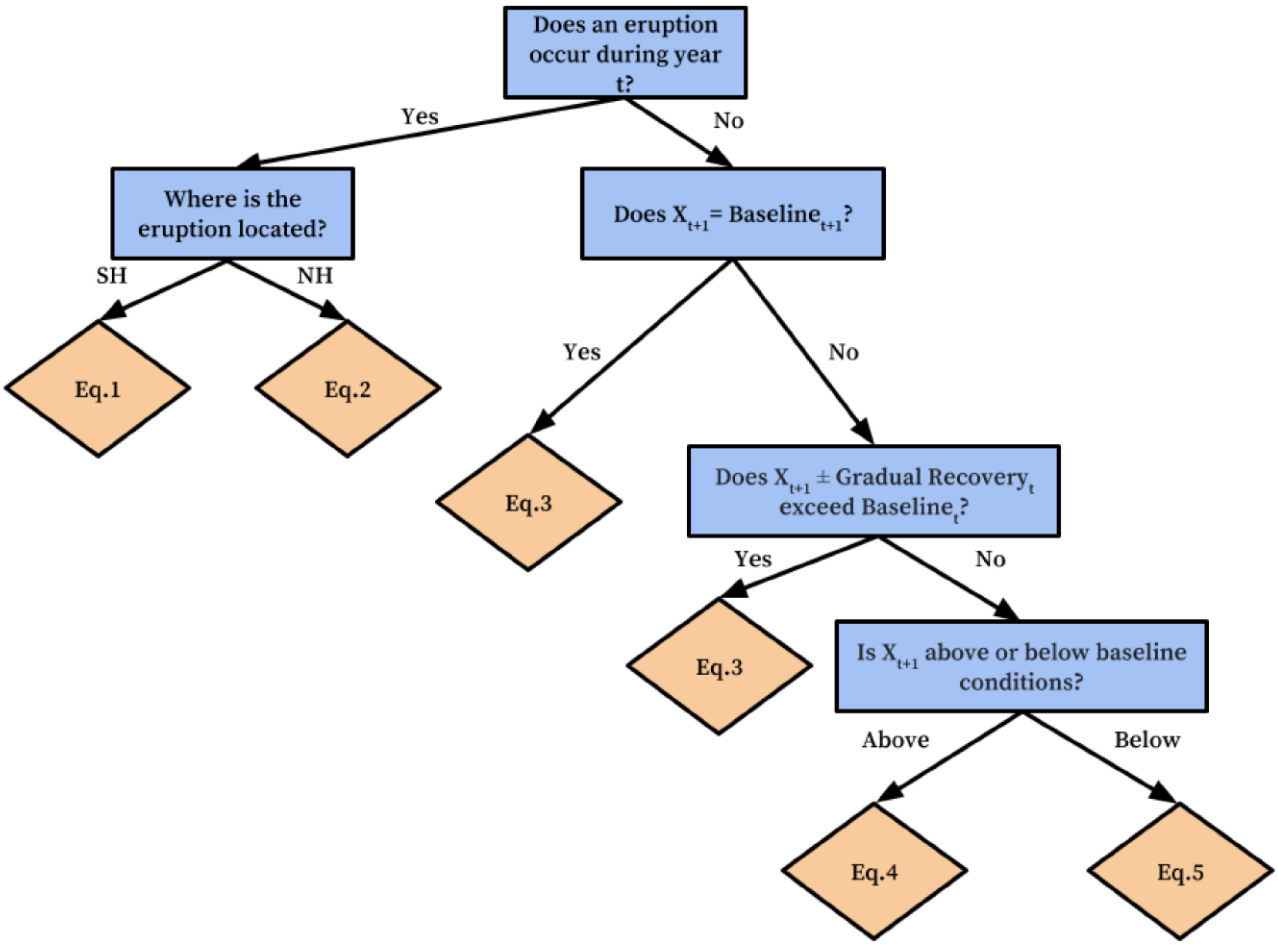

Figure 3: The statistical model decision tree algorithm with input and boundary condition dictated pathways. Equations at the end of each pathway determine the modelled $\delta^{18}O$ value for that time slice; any terms refer to those in Eq.1 – Eq.5. If t = 1000 (a BP), t+1 = 1001 (a BP).

2.1.1: Temperature Baseline *(B)*

The temperature baseline reflects the climate system in a stable and unperturbed state relative to dynamic background conditions; the model assumes that a perturbed and unstable climate system will always tend to the temperature baseline after the dissipation of perturbing climate forcing mechanisms. Although insolation is a significant influence on long-term climate and temperatures (Kukla, 1972; Berger, 1988; Felzer et al., 1998; Campisano, 2012; Croll & Sugden, 2021), insolation modulates changes in atmospheric CO_2 concentration, which then drives most of the temperature shifts (Caillon et al., 2003). Furthermore, the decoupling between insolation and global temperature - documented in proxy records in the Holocene - illustrates that in recent millennia atmospheric CO_2 concentration had more influence on long-term global climate patterns (Kuo et al., 1990; Felzer et al., 1998; Rohling et al., 2010; Pasini et al., 2012; Shakun et al., 2012; Humlum et al., 2013; Wallmann, 2014; Moossen et al., 2015; Ruddiman et al., 2016). Even though both factors influence long-term global temperatures, the NGRIP $\delta^{18}O$ Greenland temperature proxy is better defined by atmospheric CO_2 concentrations; abrupt change magnitude, timing, and frequency in the NGRIP $\delta^{18}O$ record are generally better matched by atmospheric CO_2 concentration ($R^2 = 0.63$) than insolation ($R^2 = 0.21$) over the Quaternary (Figure 4a). Furthermore, the decoupling of temperature and insolation during the late Holocene is identifiable in the NGRIP $\delta^{18}O$ record at ~8 ka BP (Figure 4b). Consequently, temperature baseline values in the statistical model paralleled atmospheric CO_2 concentration throughout; the first modelled Greenland $\delta^{18}O$ value (100 ka BP) was always

at the Greenland temperature baseline, which closely paralleled the NGRIP $\delta^{18}O$ at this time slice.

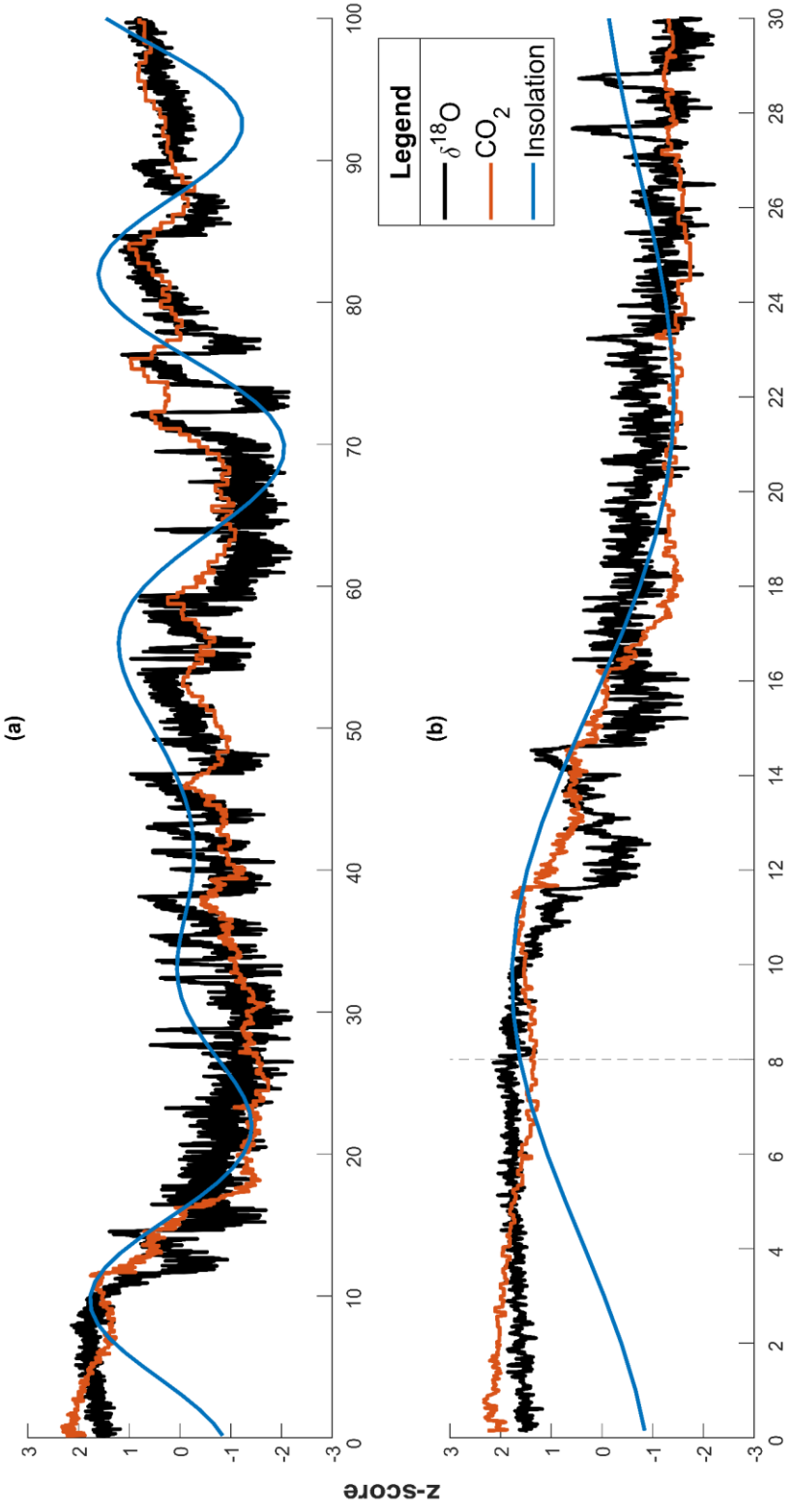

Figure 4: NGRIP $\delta^{18}O$ (black), atmospheric CO_2 concentration (orange), and insolation (blue) throughout the model time frame. Atmospheric CO_2 concentrations track NGRIP $\delta^{18}O$ values better than insolation over the entire timespan, with a reported R^2 of 0.63 for Atmospheric CO_2 concentration vs 0.21 for insolation against NGRIP $\delta^{18}O$ respectively (a). The dashed line shows that the decoupling of NGRIP $\delta^{18}O$ and insolation seems to occur somewhere around 8 ka BP, after which NGRIP $\delta^{18}O$ is much better matched by atmospheric CO_2 concentrations than insolation (b).

2.1.2: Climate Sensitivity *(n)*

Sensitivity to abrupt climate change varied throughout the Quaternary (Armour et al., 2013; McCarroll, 2015); land-based ice volume is a well-documented influence on the degree of climate change sensitivity during the Quaternary (Grant et al., 2012), because millennial-scale climate change was most likely to occur during periods of intermediate land-based ice volumes (Grigg et al., 2001; Baldini et al., 2015, 2018; Zhang et al., 2014, 2017). Therefore, a simple predictive model using sea level as a land-based ice volume indicator quantified the sensitivity to abrupt climate change annually throughout the modelled period. The model extracted NGRIP δ^{18}O standard deviation (σ) and mean average z-score normalised sea level values over windows varied by 1000 years in duration between 1000 – 10000 years. The σ value of NGRIP δ^{18}O over a given window defined the climate sensitivity of the period, where high σ values reflected a window of greater sensitivity compared to low σ values. The most appropriate time window was the window with the strongest statistical relationship alongside a lack of overfitting to the predictor variable data. The regression coefficients in an overfitted model represent noise rather than the underlying relationships of that individual dataset. As a result, generalising outside the original dataset using an overfitted model is not appropriate as the model cannot account for random noise patterns of other datasets. Using this approach, the best model was a cubic relationship with a window size of 3000 years, with a reported $R^2 = 0.35$ and p-value < 0.01 (Figure 5) (Eq.6), which took the form

$$\text{Eq.6: } Y = (a.X^3) - (b.X^2) - (c.X) + d$$

where Y is climate sensitivity, a is a constant of 0.0042 (2 s.f.), X is sea level (z-score), b is a constant of 0.10 (2 s.f.), c is a constant of 0.091 (2 s.f.), and d is a constant of 0.53 (2 s.f.).

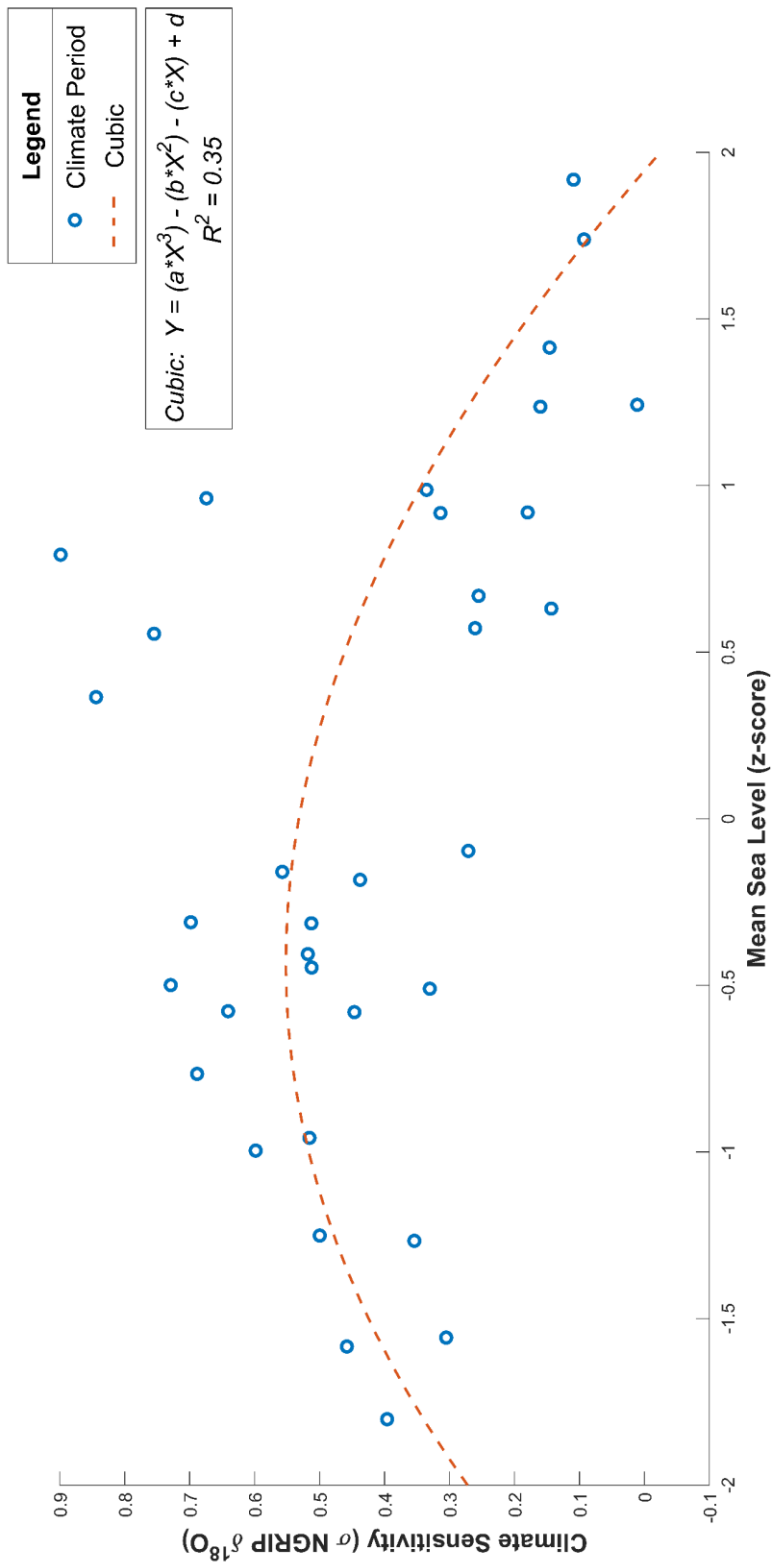

Figure 5: Cubic relationship between mean average sea level (z-score) and Climate Sensitivity (σ NGRIP $\delta^{18}O$) over 3000-year periods. Predicted sensitivity peaks between mean average z-score sea level values between -1 – 0. Past this range, climate sensitivity decreased sharply if mean average sea level increased. Recorded sensitivity varied most between mean average sea levels between 0.5 – 1.5, with a climate sensitivity range of ~0.9.

Models that used a greater window size did not have significantly higher R^2 values and introduced overfitting concerns, while models with a reduced window size had a lower R^2 values than the selected model. The interpretations made using this model are consistent with other results suggesting that climate sensitivity peaks during periods of intermediate land-based ice volumes (Grigg et al., 2001; Baldini et al., 2015, 2018; Zhang et al., 2014, 2017). Using this model, the boundary conditions at the time of an eruption had a key influence on the nature of the modelled abrupt Greenland $\delta^{18}O$ change event as volcanic eruptions of equal magnitude would not always cause an abrupt change of equal magnitude. This analysis added influential weight to the timing of explosive volcanism on the nature of modelled abrupt Greenland $\delta^{18}O$ change, reducing the likelihood of random chance causing any similarities between the NGRIP $\delta^{18}O$ and modelled Greenland $\delta^{18}O$ datasets.

2.1.3: Gradual Recovery Rate *(R)*

The gradual recovery rate (GRR) is the rate of the return of perturbed unstable temperatures to baseline stability during periods where perturbing climate forcing is absent. Temperature changes from one year to the next are small during these periods compared to large temperature changes caused by abrupt climate forcing mechanisms. As with the temperature baseline, boundary conditions influenced GRRs throughout the model period. The absorption and reemission of longwave radiation emitted by Earth's surface back into the atmosphere by greenhouse gases such as water vapour and CO_2, known as the 'Greenhouse Effect', is a crucial moderator of Earth's temperature (Bowman, 1990; Cline, 1991; Ledley et al., 1999; Lacis et al., 2010; Kweku et al., 2018). Periods of high

greenhouse gas concentrations, such as the late Holocene, have enhanced levels of the greenhouse effect, resulting in warmer conditions because of unbalanced radiative forcing; greater greenhouse gas concentrations cause more absorption and remission of longwave radiation, resulting in warmer temperatures compared to periods with lower greenhouse gas concentrations (Bowman, 1990; Cline, 1991; Ledley et al., 1999; Lacis et al., 2010; Kweku et al., 2018).

Therefore, during perturbed climate periods, the annual concentration of atmospheric greenhouse gasses is a critical control on the annual GRR. During periods of low atmospheric greenhouse gas concentrations, glacial surface mass balance tends to be more positive (Ridley et al., 2010); during such periods, GRRs are greater as melted ice regrowth in the compressed Polar cell occurs rapidly, causing the Polar cell to decompress quickly, driving the Hadley and Ferrel cells back to unperturbed positions rapidly. Consequently, the ITCZ migrates back to an unperturbed position soon after the decline of perturbing climate forcing caused by explosive volcanism. In comparison, during periods of high greenhouse gas concentrations, glacial mass balance tends to be less positive, or even negative (Ridley et al., 2010); consequently, such periods have low GRRs as ice regrowth of melted ice in the compressed Polar cell is slow, meaning that the Polar cell decompresses slowly. As a result, the Hadley and Ferrel cells return to unperturbed positions gradually, meaning the ITCZ migrates slowly back to an unperturbed position after the decline of perturbing climate forcing caused by explosive volcanism.

Using this concept, a predictive model quantified annual GRRs based on annual atmospheric CO_2 concentrations over the last 100 ka BP. Using all large magnitude DO

events that deviated from stable baseline conditions, measurements of the duration of the gradual recovery period documented in the NGRIP $\delta^{18}O$ record after each abrupt warming period allowed the extraction of a straight-line equation to describe the nature of the gradual recovery after each event. The straight-line extrapolated based on the gradual recovery rate of each period, ignoring any abrupt changes (Figure 6). After measuring the duration of the gradual recovery of each event, a cross-check quality analysis assessed the usability of each event. The analysis assigned a rank to each event (1 = unusable, 10 = very usable) based on the noise around each straight-line equation and the duration of each event. Unusable events were those with short-term periods of noisy gradual cooling (Figure 6c); Usable events were those with usability ranks ≥ 6 and straight-line relationships with a p-value < 0.0001 (Figure 6a and 6b). The atmospheric CO_2 concentration at the peak of the abrupt warming (Peak CO_2) indicated the climate boundary conditions at the onset of gradual recovery. An exponential relationship defined the relationship between GRR and Peak atmospheric CO_2 concentration best (Figure 7) (Eq.7), which took the form

$$\text{Eq. 7: } Y = (b.(X + k)^c) + d$$

where Y is the Gradual Recovery Rate (yr^{-1}), b is a constant of -0.0017 (2 s.f.), X is the Peak atmospheric CO_2 concentration (z-score), k is a constant of 2.0 (2 s.f.), c is a constant of -5.6 (2 s.f.), and d is a constant of -0.00077 (2 s.f.). Using this exponential relationship (Eq. 7), the statistical model calculated annual GRR values over the last 100 ka BP.

This analysis indicated that the highest GRR sensitivity to Peak atmospheric CO_2 was between values of 0.5 – 1 (constant k included); GRR decreased sharply with small

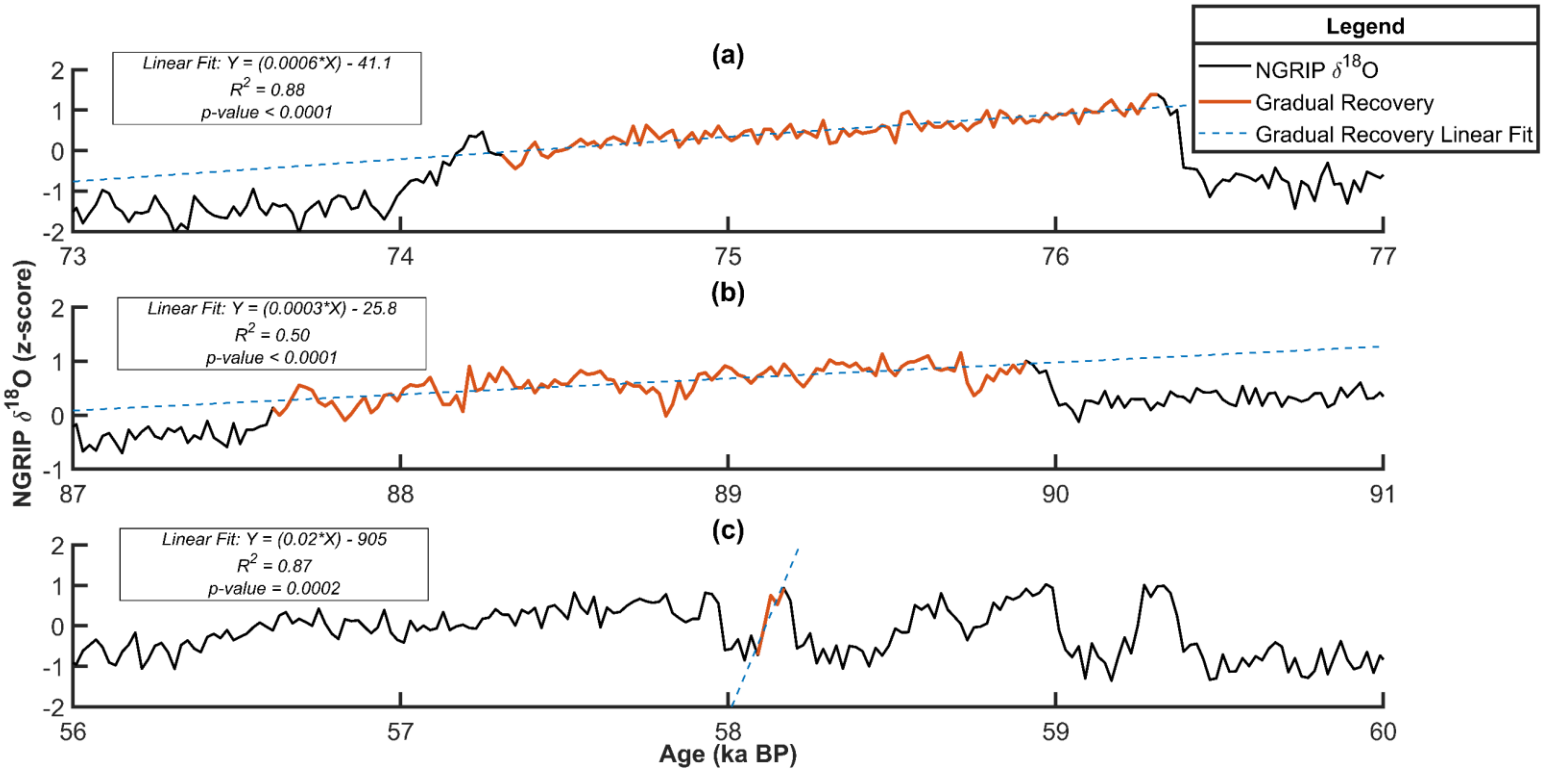

Figure 6: Gradual recovery periods of three DO events, ranging from highly usable (a), moderately usable (b), and unusable (c). The top event was the most useful (usability rank = 10) due to the statistical significance of the linear relationship, with low noise around the modelled fit (a). The middle event was moderately useful (usability rank = 6) due to increased noise around the modelled fit (b); this noise was not large enough to deem the event unusable. The bottom event was unusable (usability rank = 1), even though the linear relationship was significant, because of the short duration of the event (c); the short duration meant that confidence in distinguishing between gradual or abrupt cooling over the period was low.

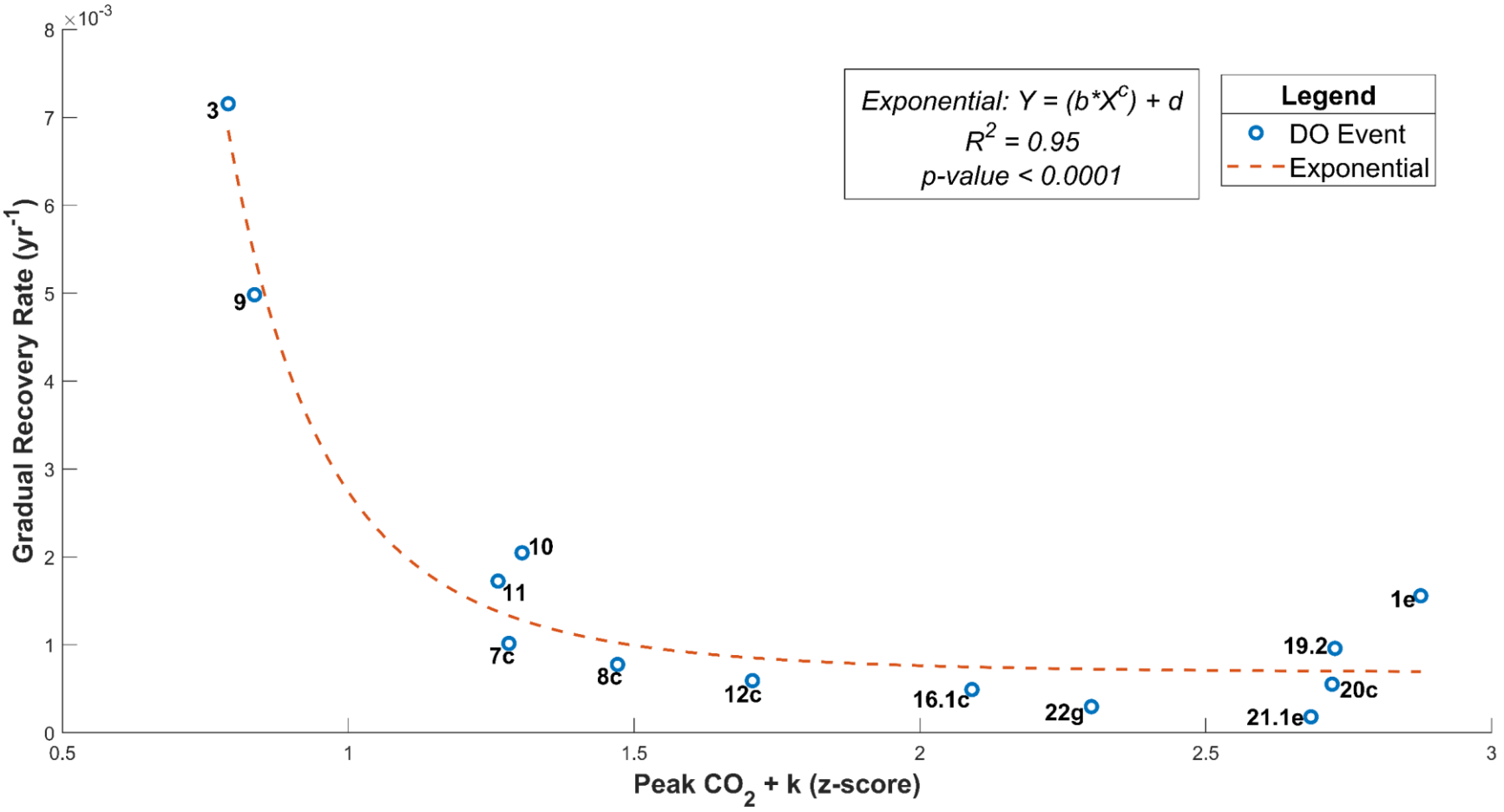

Figure 7: Exponential relationship between the GRR and Peak CO_2 value of each usable DO event. Exponential relationship fitting permitted by addition of constant k (k=2), removing negative values of Peak CO_2. The direction of the GRR depends on the recovery type of the climate period (warming = positive GRR, cooling = negative GRR). Event labels taken from Rasmussen et al. (2014).

increases in Peak atmospheric CO_2 concentrations within this range. GRR was much less sensitive to changes in Peak atmospheric CO_2 values between 1 – 1.5; GRR showed little to no sensitivity to Peak atmospheric CO_2 concentrations that surpassed a threshold value of 1.5. This analysis revealed a threshold behaviour between GRR and atmospheric CO_2 concentrations and highlighted the important influence of atmospheric greenhouse gas concentrations on the rate of return to stable temperatures. This analysis supports the concept that boundary climate conditions have an important influence on millennial-scale climate change; considering these conditions is key to understanding the nature of these events. The climate model incorporated this analysis to produce scaled and dynamic periods of gradual recovery during windows where the climate was not influenced by volcano-triggered forcing mechanisms but perturbed from baseline conditions. The model did not allow for GRR to cause fluctuations around the baseline temperature, meaning that if the GRR value surpassed the baseline in any given year, adjustments to the GRR capped the recovery at the baseline; the repetition of Eq.3 in the decision-tree algorithm ensured this (Figure 3).

2.1.4: Magnitude Constant *(u)* and Magnitude Thresholds

The climate model assumed that larger magnitude eruptions would result in larger magnitude abrupt millennial-scale climate change events. A complex relationship between eruption magnitude and radiative forcing exists; factors such as eruption latitude, eruption timing, magma type, tectonic settings, wind direction and many others influence the net radiative forcing impacts of volcanic eruptions (Sigurdsson, 1990; Scaillet et al., 1998; Bursik, 2001; Aiuppa et al., 2005; Self, 2006; Hoshyaripour et al., 2012). However, the

inferred under-recording in the known volcanic catalogue (Brown et al., 2014; Rougier et al., 2018) alongside the absence of instrumental data means the relationship between eruption magnitude and radiative forcing impacts of known eruptions over the last 100 ka BP is very ambiguous. With larger explosive volcanic eruptions tending to have larger eruption columns on average (Carey and Sigurdsson, 1989; Durant et al., 2010; Wilson et al., 1978), the model assumed that any sulphur ejected by a volcanic eruption had a greater probability of reaching the stratosphere during larger magnitude eruptions. Consequently, the model assumed that larger magnitude eruptions led to greater initial radiative cooling in the host hemisphere compared to smaller magnitude eruptions. In the context of the hypothesis underpinning the model, compared to small magnitude events, large eruptions cause more severe hemisphere temperature asymmetries because of the greater radiative cooling of the host hemisphere, leading to the ITCZ migrating further towards the warmer hemisphere, resulting in larger magnitude abrupt climate change events.

Therefore, the statistical model ensured magnitude constant values were strictly proportional to eruption magnitude. After running the 'Known Eruptions' model (see next subsection) with no magnitude constants, Excel 'Solver' calculated the constant for each magnitude to minimise the SSRs between NGRIP $\delta^{18}O$ and the modelled $\delta^{18}O$ time-series. With the magnitude constant values included, 'Solver' calculated the threshold magnitude of eruptions which minimised the SSR value between NGRIP $\delta^{18}O$ and the modelled $\delta^{18}O$ time-series. As a result, the climate model only considered SH eruptions > M5 and NH eruptions > M6 large enough to cause abrupt climate change events.

2.1.5: Statistical Model Variants and Model Output Types

The mechanics of the climate model outlined above remained consistent throughout the investigation, but the input of volcanic eruptions had four distinct variants. Model 1 ('Known Eruptions') used all known eruptions from the LaMEVE database (Crosweller et al., 2012; Brown et al., 2014) over the last 100 ka BP with medium to high dating quality, which satisfied the climate model magnitude threshold constraints (Figure 8) (Appendix 1).

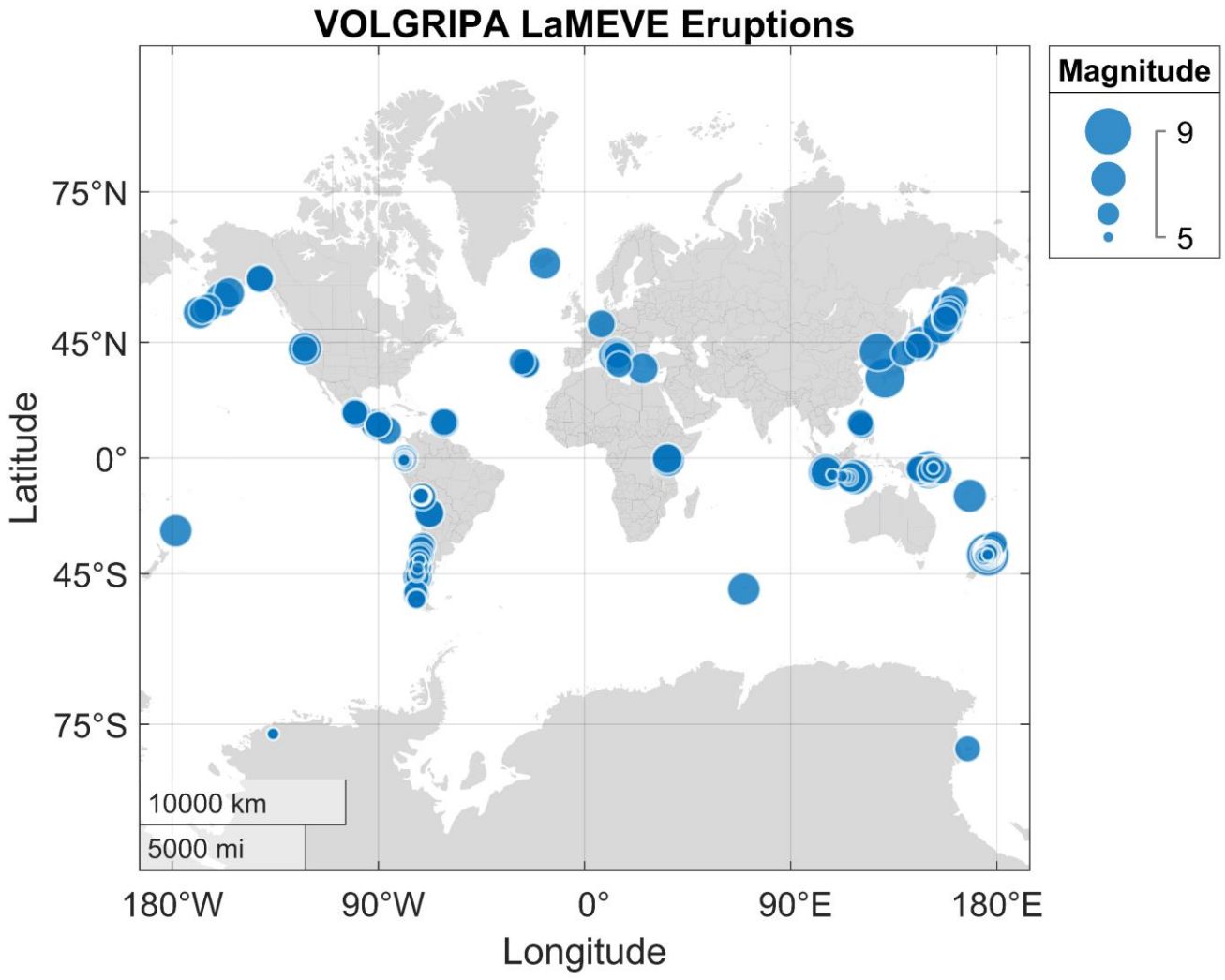

Figure 8: All known eruptions from the LaMEVE catalogue between 0 – 100,000 a BP with medium to high dating quality which satisfied the climate model magnitude thresholds.

The average volcanism during years with multiple eruptions defined the net abrupt climate forcing impact. For example, if a single year had two eruptions, one M7 (NH) and the other M5 (SH), the average would be M1 (NH) due to the opposing relationship between the eruptions; in this case, the year does not satisfy the climate model magnitude thresholds, so the model would deem it a period without abrupt climate change forcing. Model 2 ('Uniform') was an experimental model, which used a uniform distribution of random probability to assign a net volcanic forcing annually throughout the model; in this model, an M8 eruption (NH or SH) was just as likely to occur as an M1 eruption (NH or SH). Model 3 ('Weighted Probability') took a similar approach to Model 2 ('Uniform'), but instead of a uniform distribution of magnitude, annual magnitude values resulted from a weighted probability calculation. Probability values based on magnitude return periods from Rougier et al. (2018) and the hemispheric distribution split of the Model 1 eruptions (0.875(NH): 0.125 (SH)) resulted in a generated eruption time-series based on the current knowledge of volcanic distribution and frequency-magnitude behaviour (Appendix 2). With this model, an M1 (NH) eruption was much more likely to occur than an M8 (SH) eruption in any given year (Table 2). Finally, Model 4 ('Combination') used eruptions from Model 1 ('Known Eruptions') and filled in the unknown years using the same approach as Model 3 ('Weighted Probability') to produce an eruption distribution time-series with a magnitude-frequency relationship within the 95% confidence interval given by Rogier et al. (2018); therefore, Model 4 ('Combination') had the most accurate estimation of net volcanism in each year (known eruptions plus an estimate for probable 'missing eruptions'). All models that included probability-based calculations completed one million iterations, which allowed

Table 2: Return Period and Annual Exceedance Probability values derived from Rougier et al. (2018) and Model 1 eruption hemisphere distribution for magnitudes satisfying the model thresholds. Negative magnitudes represent NH eruptions; positive magnitudes represent SH eruptions.

Magnitude	Return Period (years)	Annual Exceedance Probability
-8	19400	5.15×10^{-5}
-7	1370	7.29×10^{-4}
6	880	1.14×10^{-3}
7	9600	1.04×10^{-4}
8	136000	7.35×10^{-6}

documentation of model error and success over a varied input; each iteration produced an R^2 value of modelled Greenland $\delta^{18}O$ against NGRIP $\delta^{18}O$ over the last 100 ka BP to describe reconstruction success, ultimately leading to the extraction of the single 'best' performing (highest R^2) modelled $\delta^{18}O$ time-series over the entire iteration cycle - any modelled $\delta^{18}O$ time-series discussed in subsequent sections refers to the 'best' iteration unless stated

otherwise. Graphical comparisons between the NGRIP $\delta^{18}O$ and each 'best' modelled $\delta^{18}O$ time-series supported the regression analyses by verifying the degree of reconstruction success. The statistical model could output different abrupt temperature change types, resulting from unique combinations of input eruption time-series, as well as dynamic boundary conditions at the time of eruptions altering the nature of each abrupt temperature change event (Figure 9).

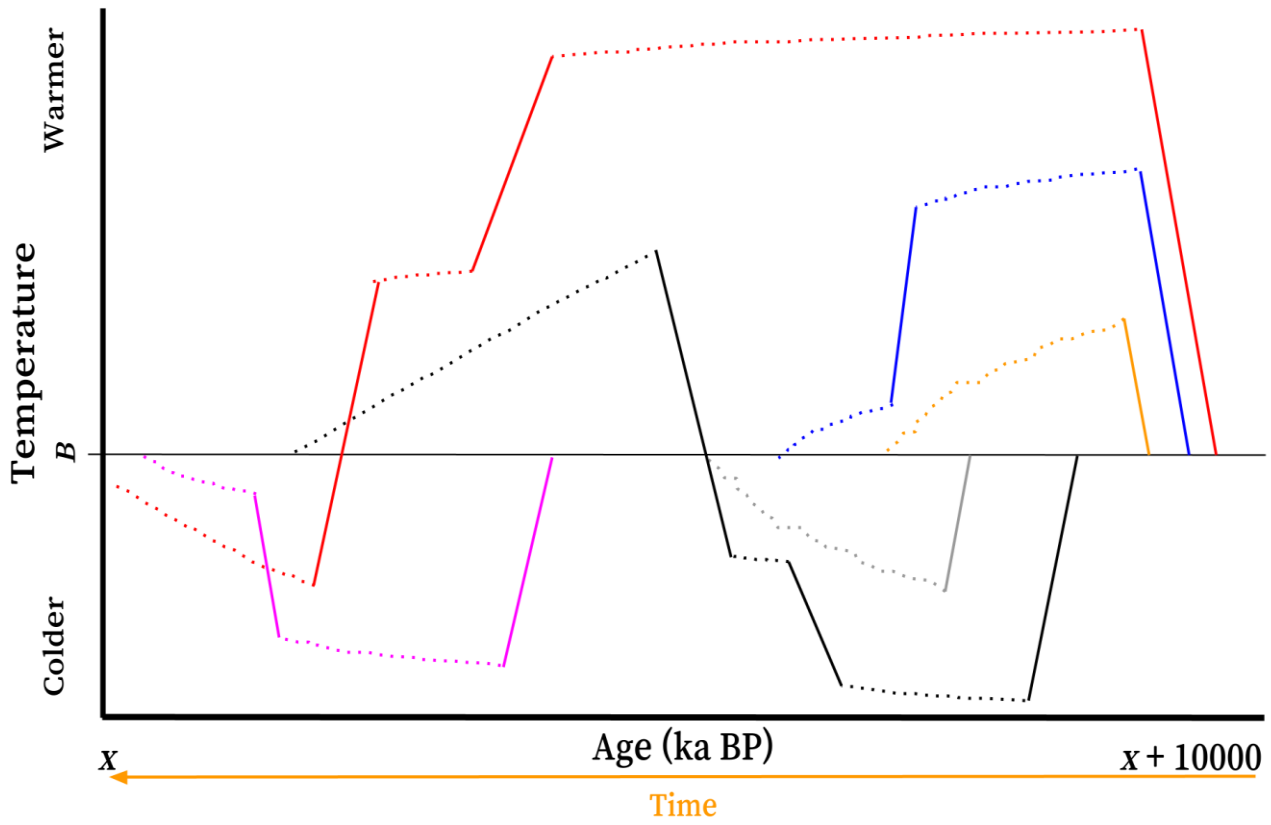

Figure 9: Schematic examples of different output types from the statistical model over any given 10,000-year window during the last 100,000 years. Each colour shows an independent event variant. For each variant, an explosive volcanic eruption triggers an abrupt Greenland temperature change (solid-coloured line) from the temperature baseline *(B)* (SH eruptions = warming, NH eruptions = cooling). Subsequent restoration of baseline conditions occurs during periods of gradual recovery (dashed-coloured lines) and abrupt temperature changes caused by explosive volcanic eruptions located in the opposing hemisphere of the initial perturbing eruption. Simple events include a single abrupt temperature change followed by a gradual recovery to the temperature baseline (orange and grey events), whereas complex events can include multiple abrupt temperature changes with intermittent periods of gradual recovery (blue and pink events), which can cause temperatures to oscillate around the temperature baseline (red and black events). Events occur in the past and develop in the direction of the present day (right to left).

Section 3: Results and Discussion

3.1: Addressing the Aim of the Investigation

The results of this investigation make a compelling case for the consideration of explosive volcanism as a potential trigger of millennial-scale climate over the last 100 ka BP. This draws on a holistic consideration of both graphical and statistical results, as there is no single test that can define the success of the statistical model variants (Martis, 2006; Ling & Mahadevan, 2013). For example, over the entire 100 ka interval, the theoretically modelled δ^{18}O time-series underpinned by volcanic magnitude-frequency statistics (Rougier et al., 2018) (Model 1 ('Known Eruptions'), Model 3 ('Weighted Probability') and Model 4 ('Combination')) showed considerable graphical and statistical similarities with the NGRIP δ^{18}O time-series (Table 3; Figure 10, 11 and 12); Periods of Interest (POIs) show windows of key similarities and differences between both time-series (Figure 10, 11 and 12). Furthermore, the percentage error distribution of each theoretically modelled output does not cause concern (Figure 13); each modelled output had a considerable proportion (>60%) of error within the ±100% of the true NGRIP δ^{18}O time-series value (Table 4). Accounting for the extensive time frame and the sensitivity of each model to annual eruption timing and magnitude, these errors indicate a good performance overall. These results suggest that explosive volcanism is a feasible potential trigger of millennial-scale climate change. The weak performance of the Model 2 ('Uniform') δ^{18}O time-series highlights the importance of acknowledging volcanic magnitude-frequency statistics when investigating the relationship between explosive volcanism and millennial-scale climate change (Rougier et al., 2018). For example, little to no graphical or statistical similarity

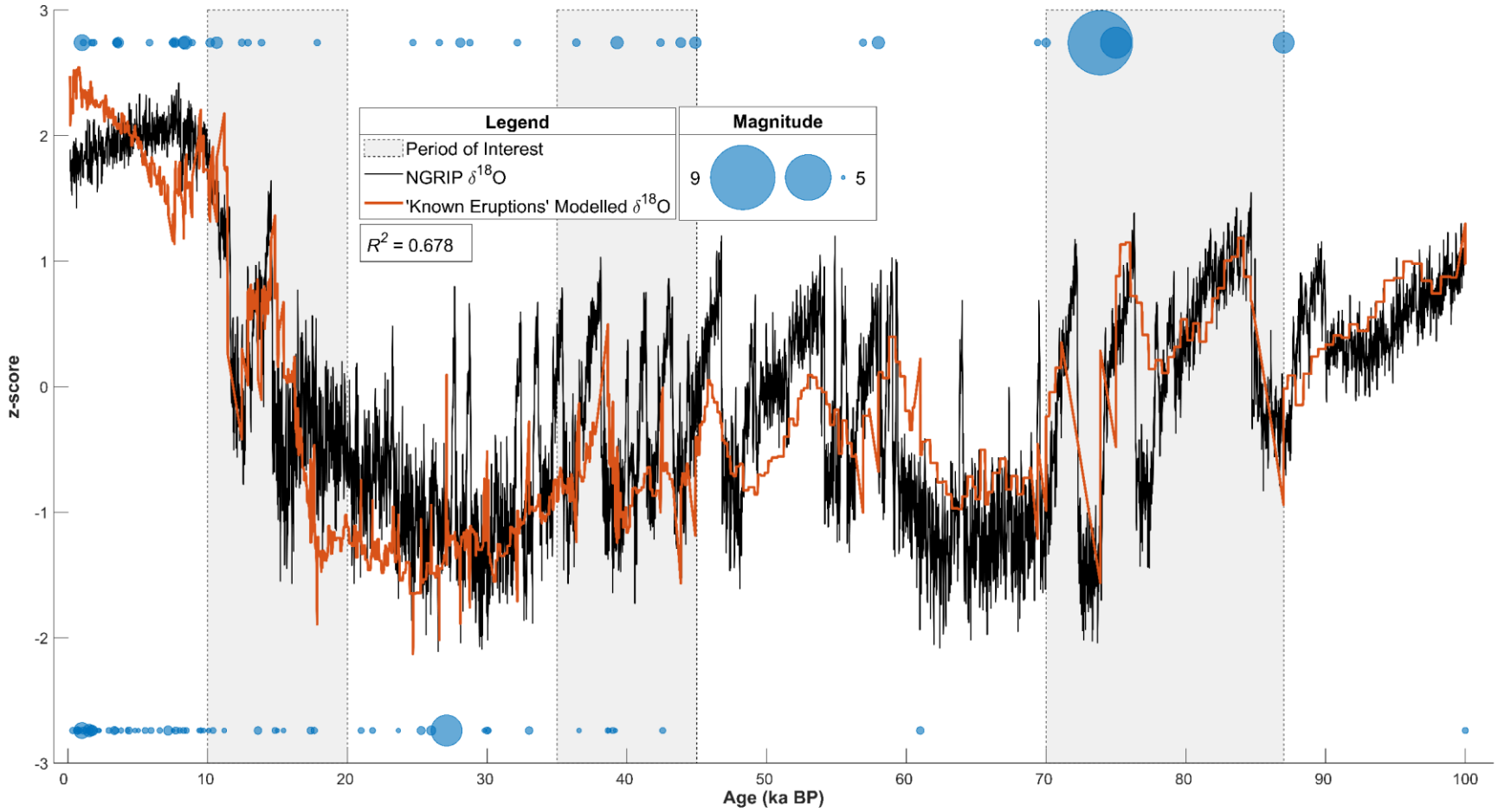

Figure 10: 'Known Eruptions' modelled δ^{18}O time-series and NGRIP δ^{18}O time-series between 0 – 100 ka BP. Grey zones highlight POIs, where key visual similarities or differences between the two time-series exist. Blue bubbles represent the volcanic time-series used by the model. Bubbles in the top half of the figure are NH eruptions; bubbles in the bottom half are SH eruptions.

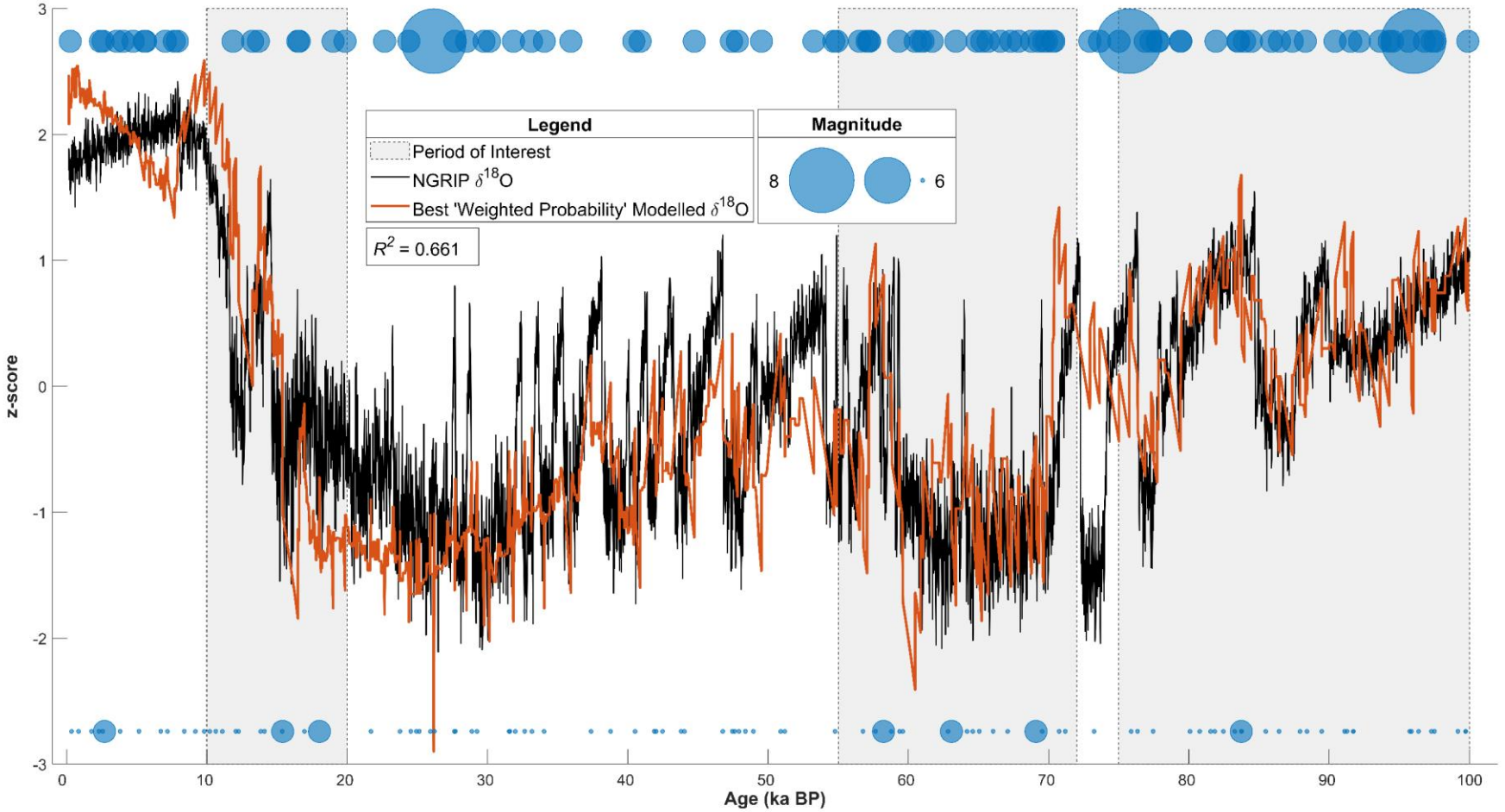

Figure 11: 'Weighted Probability' modelled $\delta^{18}O$ time-series and NGRIP $\delta^{18}O$ time-series between 0 – 100 ka BP. Grey zones highlight POIs, where key visual similarities or differences between the two time-series exist. Blue bubbles represent the volcanic time-series used by the model. Bubbles in the top half of the figure are NH eruptions; bubbles in the bottom half are SH eruptions.

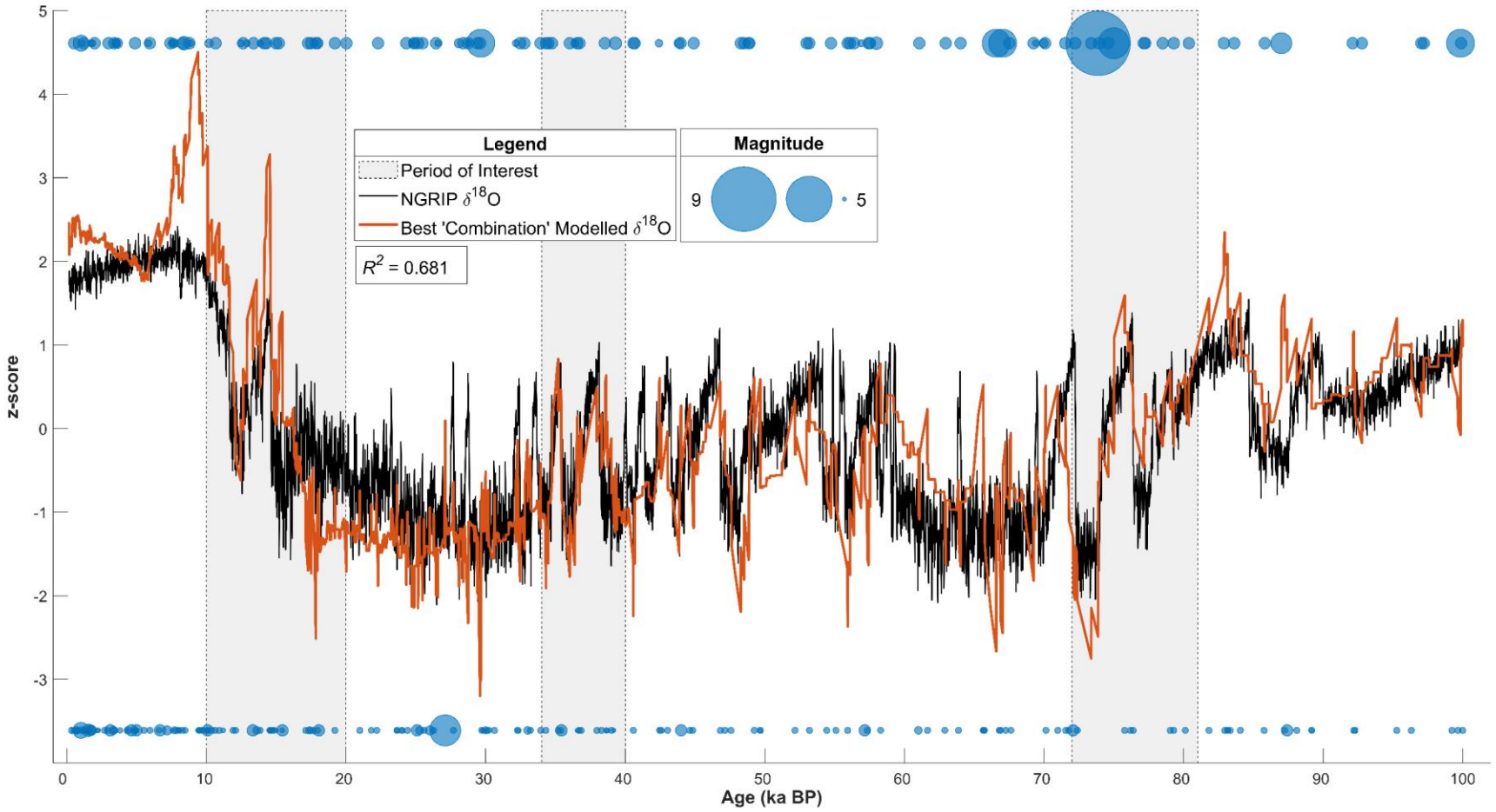

Figure 12: 'Combination' modelled $\delta^{18}O$ time-series and NGRIP $\delta^{18}O$ time-series between 0 – 100 ka BP. Grey zones highlight POIs, where key visual similarities or differences between the two time-series exist. Blue bubbles represent the volcanic time-series used by the model. Bubbles in the top half of the figure are NH eruptions; bubbles in the bottom half are SH eruptions.

Table 3: Key statistics from the linear regression between each modelled $\delta^{18}O$ time-series and the NGRIP $\delta^{18}O$ time-series. POI 1 = youngest POI shaded in corresponding modelled output graph; POI 3 = oldest POI shaded in corresponding modelled output graph.

Statistic		(Best) Modelled $\delta^{18}O$ Time-Series												
		'Known Eruptions'				'Weighted Probability'				'Combination'				'Uniform'
		Entire Window	POI 1	POI 2	POI 3	Entire Window	POI 1	POI 2	POI 3	Entire Window	POI 1	POI 2	POI 3	Entire Window
Linear Regression	R^2	0.678	0.495	0.041	0.497	0.661	0.617	0.277	0.388	0.681	0.612	0.440	0.570	0.073
	r	0.82	0.70	0.20	0.61	0.81	0.79	0.53	0.62	0.83	0.78	0.66	0.75	0.27
	p	< 0.001	< 0.001	< 0.001	< 0.001	< 0.001	< 0.001	< 0.001	< 0.001	< 0.001	< 0.001	< 0.001	< 0.001	< 0.001
	n	99860	10000	10000	17000	99860	10000	17000	25000	99860	10000	6000	9000	99860

Table 4: Percentage error descriptive statistics of each modelled $\delta^{18}O$ time-series.

(Best) Modelled $\delta^{18}O$ Time-Series	Percentage Error Statistic									
	Largest Overestimation	Largest Underestimation	IQR Band				±100% Band			
			Mean	σ	Median	Skew	Percentage of Error in Band	Mean	σ	Median
'Known Eruptions'	$2.78x10^5$	$2.86x10^5$	-14.3	29.1	-12.0	-0.22	66	-5.4	45.3	-5.4
'Uniform'	$1.61x10^9$	$6.25x10^8$	$-1.06x10^4$	$3.41x10^{20}$	$-1.95x10^4$	0.03	0.07			
'Weighted Probability'	$1.27x10^6$	$2.94x10^5$	-7.97	30.5	-5.25	0.27	65	-1.66	45.5	-0.48
'Combination'	$8.26x10^5$	$5.69x10^5$	-3.23	37.4	7.88	-0.34	62	6.22	49.9	10.7

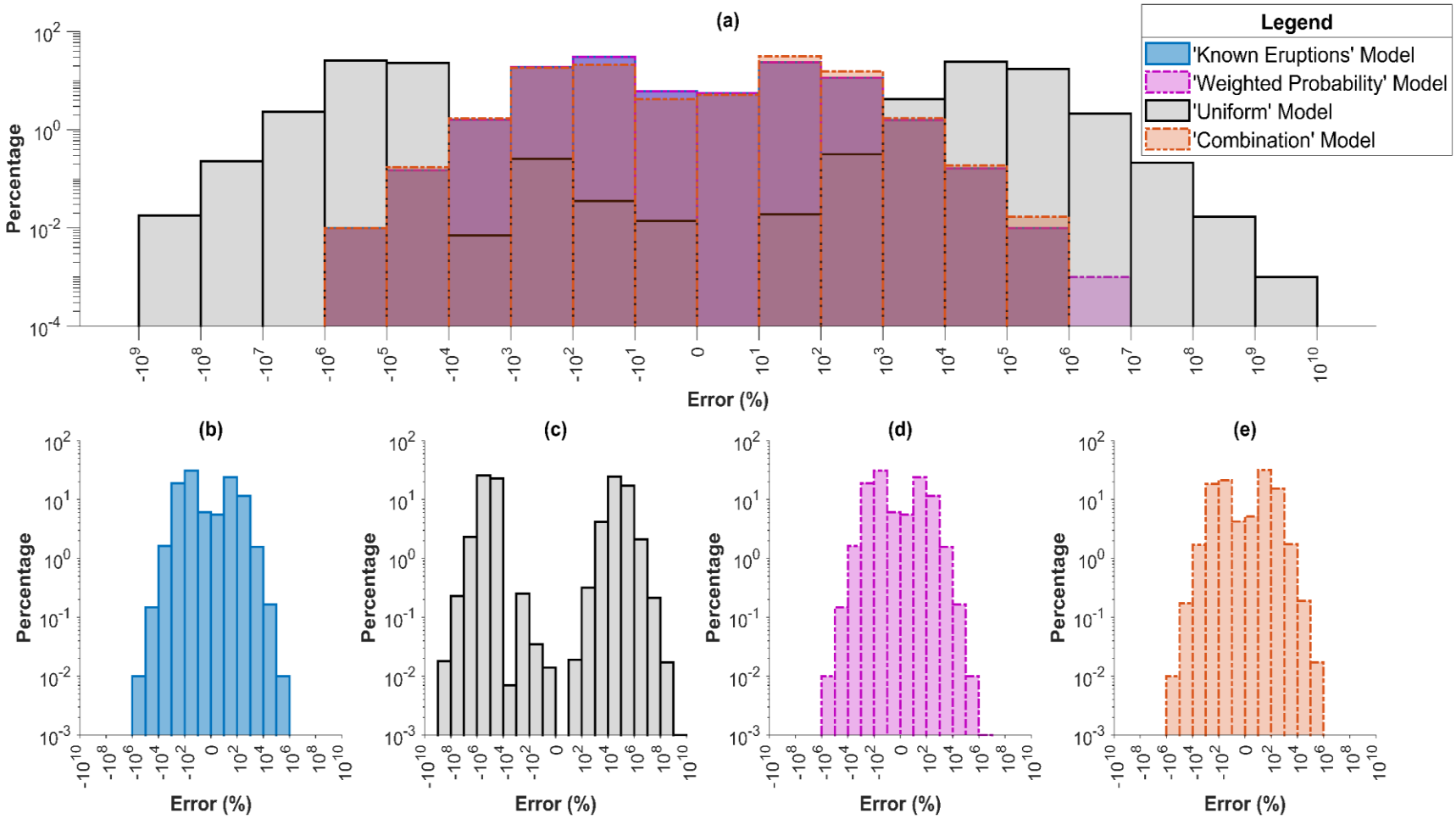

Figure 13: (a) Comparison of varied modelled $\delta^{18}O$ time-series error distributions (where $-10^2 = -1x10^2$). (b) 'Known Eruptions' modelled $\delta^{18}O$ time-series error distribution. (c) 'Uniform' modelled $\delta^{18}O$ time-series error distribution. (d) 'Weighted Probability' modelled $\delta^{18}O$ time-series error distribution. (e) 'Combination' modelled $\delta^{18}O$ time-series error distribution.

between the Model 2 ('Uniform') and the NGRIP δ^{18}O time-series exists (Table 3; Figure 14). In addition, the percentage error values for this model are problematic, as a considerably small proportion (0.07%) of the percentage error fell within $\pm$100% of the true NGRIP δ^{18}O time-series value compared to the theoretical modelled outputs (Table 4).

This result concurs with the wider literature investigating the relationship between volcanism and millennial-scale climate change. For example, previously reported statistically significant relationships between the timing of explosive volcanism and millennial-scale climate change (Bay et al., 2004; Baldini et al., 2015; Lohmann & Svensson, 2020) have suggested that explosive volcanism is closely linked to millennial-scale climate change. Of the results here, the strong similarities between the NGRIP δ^{18}O and the theoretically modelled δ^{18}O time-series strongly supports the hypothesis that explosive volcanism could trigger millennial-scale climate change through global atmospheric reorganisation (Baldini et al., 2015), and is consistent with the finding that an external random stationary process forced DO events (Lohmann and Ditlevsen, 2018). This investigation considers the inferred undercount in the volcanological catalogue (Brown et al., 2014; Baldini et al., 2015; Kiyosugi et al., 2015; Cooper et al., 2018; Papale, 2018; Rougier et al., 2018; Lohmann & Svensson, 2020) by generating statistically robust eruption time-series in Model 3 ('Weighted Probability') and Model 4 ('Combination') (Section 2.1.5) ('List of Abbreviations', p. 5). The results strongly suggest that 'missing' eruptions could have triggered millennial-scale climate change (Baldini et al., 2015); for example, the Model 4 ('Combination') time-series strongly reproduced GI-8c and GI-7c (Rasmussen et al., 2014) (Figure 12; POI 2), which Model 1 ('Known Eruptions') failed to reproduce.

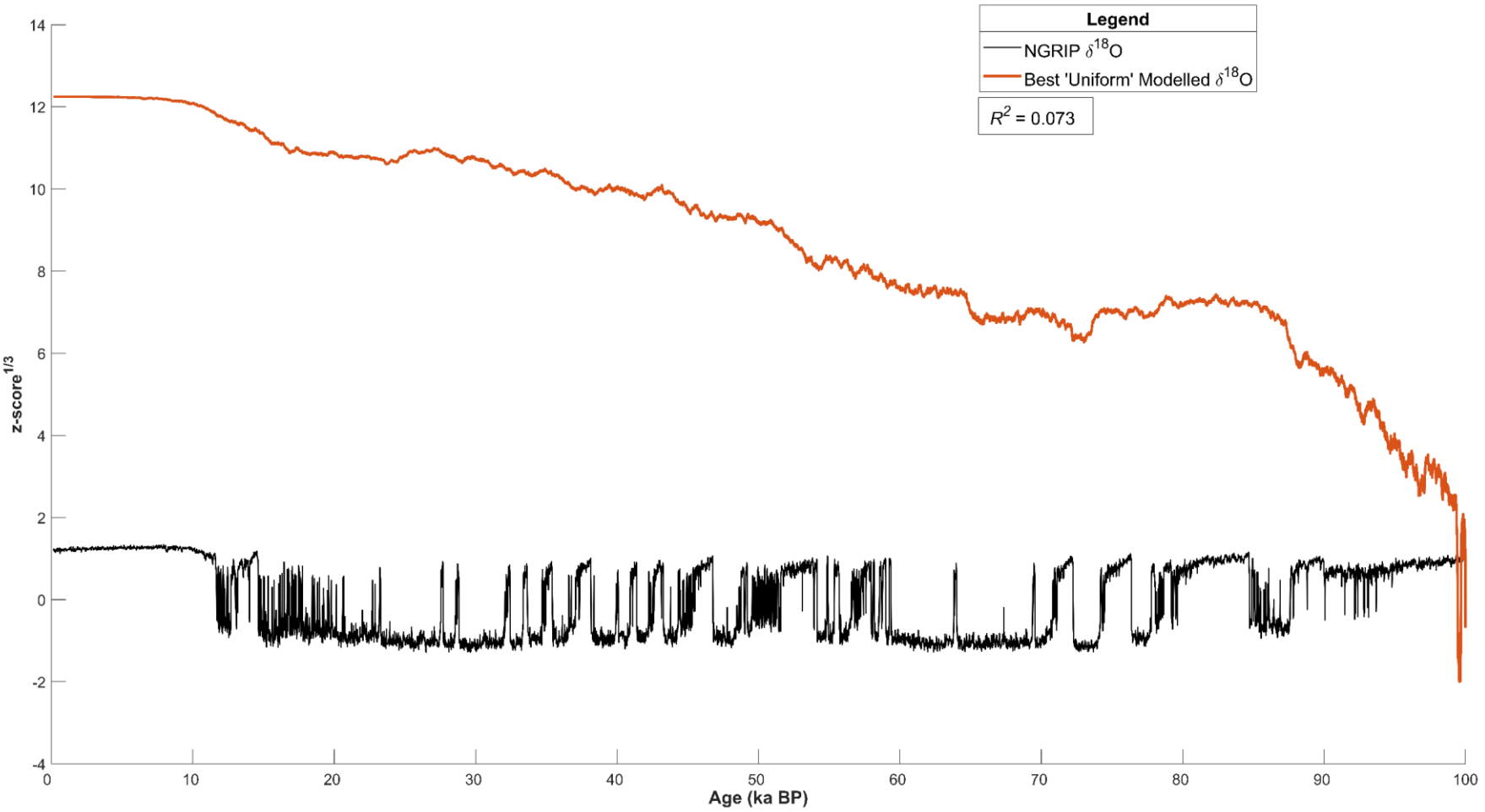

Figure 14: Best 'Uniform' modelled $\delta^{18}O$ time-series and NGRIP $\delta^{18}O$ time-series between 0 – 100 ka BP. Transformation applied to the z-scores to maximise visual clarity between the two time-series.

3.2: The Abrupt BA-YD Transition

All theoretically modelled δ^{18}O time-series reproduced the NGRIP δ^{18}O time-series well over the BA-YD transition (Figures 10, 11 and 12: youngest POI; Table 3: POI 1). The fewer eruptions in the Model 1 ('Known Eruptions') volcanic time-series could have led to a more muted reproduction of the NGRIP δ^{18}O time-series and caused the lower R^2 value (0.495) between Model 1 ('Known Eruptions') and the NGRIP δ^{18}O time-series, compared to the higher R^2 values for the Model 3 ('Weighted Probability') and Model 4 ('Combination') outputs which had statistically generated volcanic time-series (Table 5 and Figure 15). Both Model 1 ('Known Eruptions') and the Model 4 ('Combination') δ^{18}O time-series support volcanism as the trigger for the abrupt BA-YD transition. The large (M6.2) and high-sulphur Laacher See Eruption (LSE) was previously proposed as a plausible trigger of the BA-YD transition (Baldini et al., 2018). Until recently, 12.880 ± 0.040 ka BP was the widely accepted date of the LSE (Baldini et al., 2018; Bronk Ramsey et al., 2015; Lane et al., 2015). However, a new radiocarbon-based age places the LSE at 13.006 ± 0.009 ka BP (Reinig et al., 2021), apparently precluding a direct link between the LSE and the BA-YD transition (Abbott et al., 2021; Reinig et al., 2021). Nevertheless, recent research identified an extremely large sulphur spike within the NGRIP ice core occurring precisely at GS-1 cooling onset, also coinciding with the 12.880 ka BP age for the LSE (Cheng et al., 2020; Abbott et al., 2021), suggesting that the Brauer et al. (2008) age for the LSE may in fact be correct. Regardless of whether that sulphur spike represents the LSE, a very large NH eruption apparently occurred at 12.870 ka BP, and volcanism therefore remains a possible trigger

Table 5: Descriptive statistics for the volcanic eruptions used to trigger abrupt climate change in each modelled $\delta^{18}O$ time-series.

(Best) Modelled $\delta^{18}O$ Time-Series	Eruption Magnitude Distribution Statistic											
	Eruption Count		Median		Mode		Maximum		Mean		σ	
	NH	SH	NH	SH	NH	SH	NH	SH	NH	SH	NH	SH
'Known Eruptions'	37	62	6.4	6.0	6.2	6	8.8	8.1	6.6	6.0	0.61	0.58
'Uniform'	16589	22100	7.5	7.0	8.6	6.9	9.0	9.0	7.5	7.0	0.86	1.14
'Weighted Probability'	91	105	7.0	6.0	7.0	6.0	7.0	7.0	7.0	6.1	0.18	0.25
'Combination'	122	177	7.0	6.0	7.0	6.0	8.8	8.1	6.9	6.1	0.42	0.44

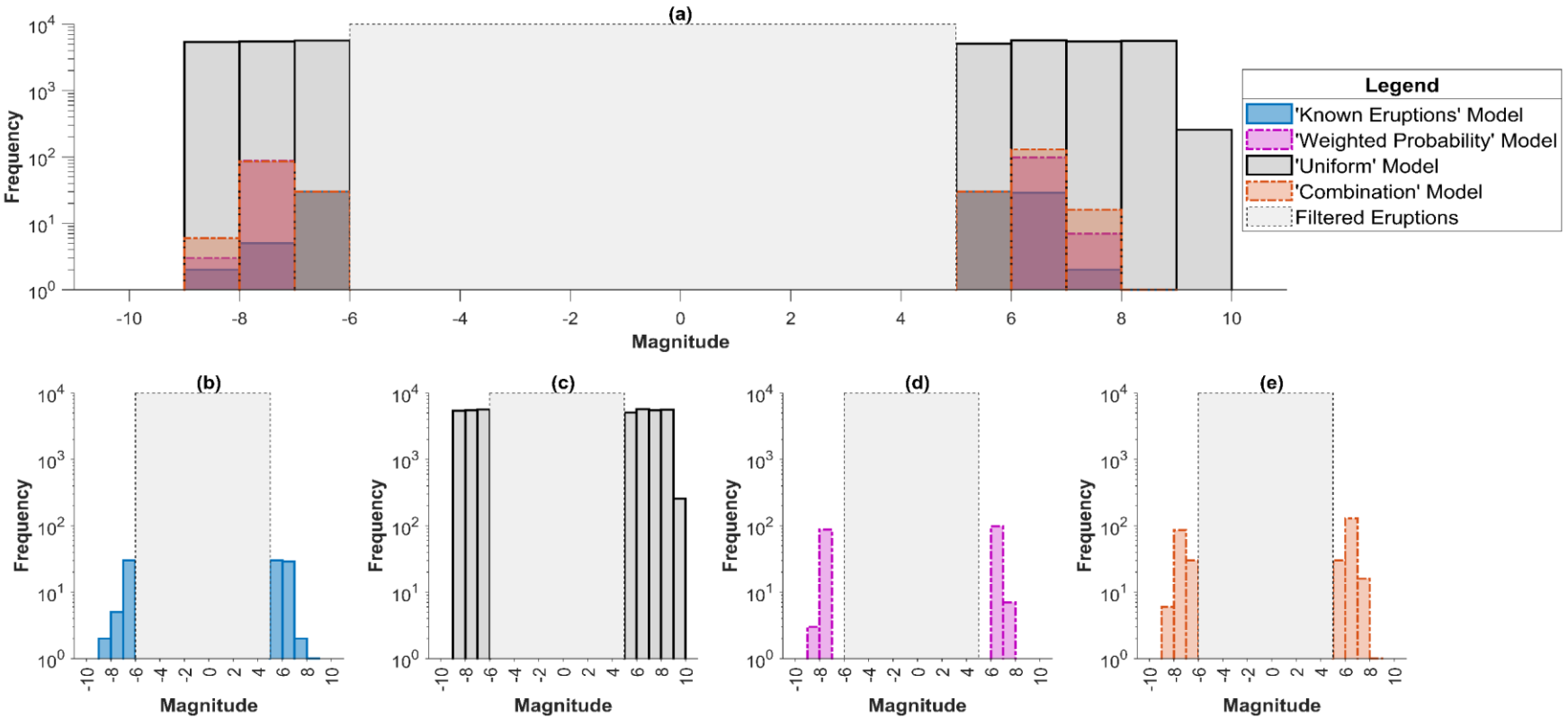

Figure 15: (a) Comparison of varied modelled $\delta^{18}O$ time-series eruption distributions. Positive magnitude values represent SH eruptions; negative magnitude values represent NH eruptions. The shaded grey area shows the eruption magnitude range filtered by the statistical model. (b) 'Known Eruptions' modelled $\delta^{18}O$ time-series eruption distribution. (c) 'Uniform' modelled $\delta^{18}O$ time-series eruption distribution. (d) 'Weighted Probability' modelled $\delta^{18}O$ time-series eruption distribution. (e) 'Combination' modelled $\delta^{18}O$ time-series eruption distribution.

of the BA-YD transition according to the sulphur record (Abbott et al., 2021). Furthermore, the reproduction of the abrupt BA-YD transition by the Model 3 ('Weighted Probability') modelled δ^{18}O time-series (Figure 11: youngest POI), with its independent statistically generated volcanic time-series, supports the consideration of any large eruption during that time as a potential trigger of the YD. As a result, the suggested consideration of an explosive volcanic eruption as a potential trigger of the abrupt BA-YD transition remains an important result (Baldini et al., 2018; Abbott et al., 2021), despite the Model 1 ('Known Eruptions') and Model 4 ('Combination') modelled δ^{18}O time-series relying on a disputed date of the LSE (Baldini et al., 2018; Abbott et al., 2021; Reinig et al., 2021).

3.3: Volcanic Origin of Greenland Stadial 20

Both the Model 1 ('Known Eruptions') and Model 4 ('Combination') modelled δ^{18}O time-series show considerable graphical and statistical similarities with the NGRIP δ^{18}O time-series over the GS-20 onset period (Figures 10 and 12: oldest POI; Table 3; POI 3). The lack of a known NH eruption coinciding with the GS-21.1 onset (Rasmussen et al., 2014) lowers the statistical performance between the NGRIP δ^{18}O time-series and Model 1 ('Known Eruptions') modelled δ^{18}O time-series over the broader period (Table 3: POI 3), but this does not impact the strong graphical reproduction of the narrower abrupt GS-20 transition (Figure 10; oldest POI). Both the Model 1 ('Known Eruptions') and Model 4 ('Combination') modelled δ^{18}O time-series rely on the M8.8 Youngest Toba Tuff (YTT) eruption (Sumatra) dated at 73.88 ±0.32 ka BP (Storey et al., 2012) and the M8.1 Los Chocoyos eruption of the Atitlán volcano (Guatemala) recently re-dated to 75 ±2 ka BP (Cisneros de León et al., 2021b). The ~1,000-year gap between each eruption is particularly noteworthy, as super-

eruption doublets are extremely rare (Rougier et al., 2018; Paine et al., 2021). Over a single iteration, the chance of Model 3 ('Weighted Probability') or Model 4 ('Combination') generating two M8 eruptions within a 1,000-year window at any point over 100,000-years is ~0.04%; therefore, the chance of a single iteration of Model 3 ('Weighted Probability') generating two M8 eruptions within ~1,000 years at the onset of GS-20 within a generated volcanic time-series that performed well over the entire 100,000-year time frame is small. Consequently, it was extremely unlikely that Model 3 ('Weighted Probability') would reproduce GS-20 over one million iteration cycles relying on the current knowledge of volcanic magnitude-frequency relationships (Rougier et al., 2018); this offers a reasonable explanation for why the Model 3 ('Weighted Probability') modelled $\delta^{18}O$ time-series performed well over this period but did not reproduce GS-20 (oldest POI; Figure 11). As a result, abrupt millennial-scale climate change events not successfully reproduced by the models (e.g., GI-18) may simply reflect unknown clusters of eruptions.

Most investigations exploring volcanism as a potential GS-20 trigger focus solely on the YTT eruption ~74 ka BP because the previous 84 ka BP date of the Los Chocoyos eruption (Drexler et al., 1980) placed the eruption well before GS-20. Some investigations make a case for considering the Toba eruption phases as a trigger for GS-20 (Zielinski et al., 1996), but others debate the role of Toba in driving GS-20 when considering climate modelling outputs and dating and sulphur load uncertainties (Oppenheimer, 2002; Robock et al., 2009; Williams et al., 2009; Polyak et al., 2017; Crick et al., 2021; Paine et al., 2021). For example, some investigations suggest that the Toba eruption phases amplified GS-20 to extremely severe conditions rather than triggering the abrupt cooling (Baldini et al., 2015; Crick et al.,

2021). This is a vitally important suggestion in the context of the new date of the Los Chocoyos eruption, as it introduces the possibility that GS-20 relied on a supereruption doublet to trigger and amplify the extreme conditions of the period (Cisneros de León et al., 2021; Paine et al., 2021), a perspective supported by both previous results that a doublet eruption event during the Holocene triggered climatic impacts (Toohey et al., 2016; Cisneros de León et al., 2022) and the results of this investigation. The dating uncertainties of the two eruptions overlap, currently preventing an accurate reconstruction of the series of events leading up to GS-20 (Cisneros de León et al., 2021; Paine et al., 2021). Regardless, this investigation supports the recent suggestion that a supereruption doublet requires consideration when looking at the potential triggers and amplification of GS-20 (Baldini et al., 2015; Paine et al., 2021), which would also explain why previous modelling attempts using only the Toba eruption ~74 ka BP could not trigger and sustain GS-20 (Robock et al., 2009).

3.4: Cross Model Comparisons

The statistical approach addressing the volcanic catalogue's inferred undercount improved modelling performance over the 100,000-year time frame. Over the entire range of errors, there was no significant difference between the average error across all modelled δ^{18}O time-series at the 95% confidence interval (Welch's ANOVA: $F = 1.28$, $p = 0.28$); post hoc analysis with a Bonferroni adjustment to reduce the probability of a Type I error (McEwan, 2017) revealed that this was consistent when comparing all modelled δ^{18}O time-series individually ($p > 0.05$ in all cases). However, within the IQR of error, a significant difference between average errors across all modelled δ^{18}O time- series exists (Welch's ANOVA: $F =$

2.81×10^3, $p < 0.001$); post hoc analysis with a Bonferroni adjustment revealed that the Model 4 ('Combination') output reproduced the NGRIP $\delta^{18}O$ time-series significantly better than any other model on average ($\mu = 3.23\%$, $p < 0.001$ in all cases). Furthermore, there was a significant difference in the average R^2 produced over one million iterations of Model 2 ('Uniform'), Model 3 ('Weighted Probability'), and Model 4 ('Combination') (Welch's ANOVA: $F = 2.13 \times 10^7$, $p < 0.001$); post hoc analysis with a Bonferroni adjustment revealed that Model 4 ('Combination') produced significantly higher R^2 values than any other model on average ($\mu = 0.443$, $p < 0.001$ in all cases). Moreover, the Model 4 ('Combination') output produced the single highest R^2 value over the entire 100,000-year time frame (Figure 16; Table 3).

Graphically, the Model 3 ('Weighted Probability') and Model 4 ('Combination') modelled $\delta^{18}O$ time-series reproduce the erratic nature of the NGRIP $\delta^{18}O$ time-series better than the Model 1 ('Known Eruptions') modelled $\delta^{18}O$ time-series. The Model 1 ('Known Eruptions') output is more muted in general, especially between 45 – 100 ka BP (Figure 10, 11 and 12). The fact that Model 4 ('Combination') outperformed Model 1 ('Known Eruptions') statistically and graphically suggests that the weighted probability approach to address the inferred undercounts in the volcanic catalogue is effective; the combination of the known volcanic catalogue with the generation of statistically-grounded 'missing' eruptions considerably enhanced the explanatory power of explosive volcanism in terms of catalysing millennial-scale climate change over the last 100 ka BP. However, the Model 4 ('Combination') $\delta^{18}O$ time-series produced some considerable overestimations of the

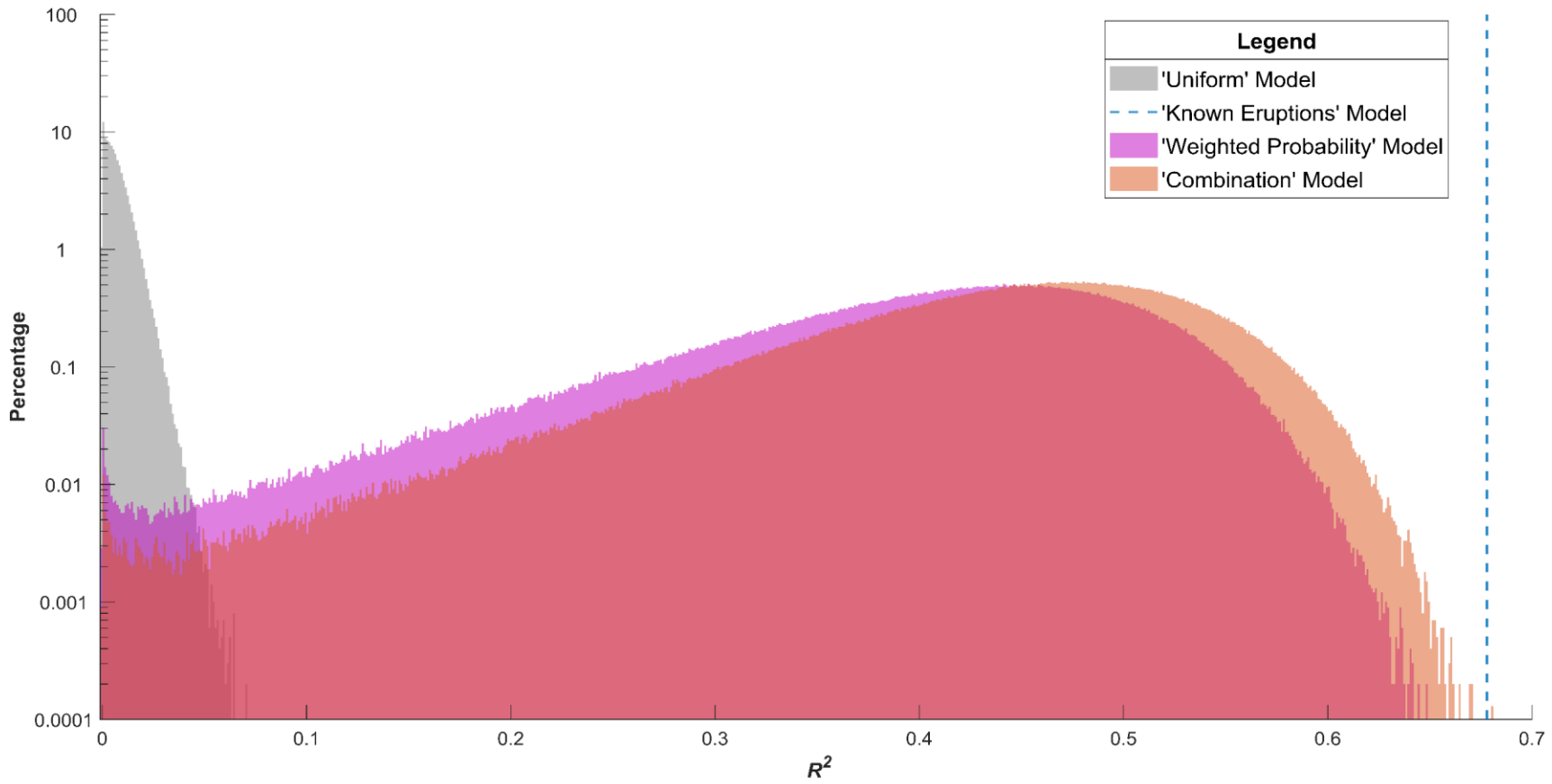

Figure 16: R^2 distributions of simple linear regressions between the NGRIP $\delta^{18}O$ time-series and the varied 'Uniform', 'Weighted Probability' and 'Combination' modelled $\delta^{18}O$ time-series over one million iterations. The R^2 of the single linear regression between the 'Known Eruptions' modelled $\delta^{18}O$ time-series and the NGRIP $\delta^{18}O$ time-series displayed.

NGRIP $\delta^{18}O$ time-series (Section 3.1.2 and Figure 12). Therefore, it is important to acknowledge that, even though the weighted probability approach to generating 'missing' eruptions has merit, it has the potential to produce anomalies with sizable errors, even in well-performing $\delta^{18}O$ time-series. However, these over-estimations were caused by the coincidence of more than one large eruption, some of which were randomly generated and may not have occurred at that time. Significantly, this observation supports the previous contention that GS-20 (which was particularly severe) was triggered by a super-eruption doublet.

This observation is also significant in the context of the wider literature. For example, it provides a developed statistical grounding supporting the hypothesis that it is likely that 'missing' eruptions in the volcanic catalogue could explain some periods of abrupt climate change (Baldini et al., 2015). Furthermore, this research underscores the importance of considering possible rare but high impact large magnitude volcanic eruptions in climate forecasting and hazard planning (Papale, 2018; Rougier et al., 2018), because these eruptions triggered the most severe abrupt millennial-scale climate change across all modelled outputs. Finally, this research illustrates how identifying and dating eruptions is vital for better understanding the impacts of volcanism, including quantifying climate effects and for evaluating risks associated with eruption return periods. The improved date of the Los Chocoyos eruption exemplifies this by offering a new reasonable explanation to counter the previous negation of the potential that explosive volcanism triggered GS-20 (Paine et al., 2021).

3.5: Limitations

A limitation of this investigation was the existence of slight offsets between some modelled outputs and the NGRIP $\delta^{18}O$ time-series over abrupt climate change periods, limiting the statistical significance. The abrupt climate change period reproduced by Model 1 ('Known Eruptions') ~39 ka BP illustrates this issue (middle POI; Figure 10); the abrupt climate change nature was well reproduced by triggers such as the Campanian eruption at 40 ± 0.1 ka BP (Fedele et al., 2008), but it is offset from the NGRIP $\delta^{18}O$ time-series by ~1,000 years. Graphically, identifying and considering this offset is straightforward. However, the regression analysis relied on the modelled and NGRIP $\delta^{18}O$ time-series being almost perfectly coincident for a strong statistical reproduction of each abrupt climate change event. The regression analysis reports a poor performance for events that are not perfectly coincident, as revealed by the poor statistical performance of Model 1 ('Known Eruptions') over 35-45 ka BP (POI 2; Table 3). As a result, between 35-45 ka BP, the graphical and the statistical results for Model 1 ('Known Eruptions') produce inconsistent reports of model success. Considering eruption dating uncertainties could maximise the correlation between the two-time series and offer a solution to this issue.

Another limitation of this investigation was calculating the iteration cycle performance over 100 ka BP; calculating performance over this long period disproportionately favoured the reproduction of abrupt climate change events which required single, highly probable eruptions compared to those which required rare clusters of large magnitude eruptions, such as GS-20 (Section 3.3). As a result, the feasibility of explosive volcanism as a potential trigger of abrupt millennial-scale climate change at individual event level requires further

investigation. A solution for this issue could involve running additional iteration cycles over short windows which have known abrupt millennial-scale climate change events. This would provide a more equally weighted investigation of the feasibility of volcanism as the potential trigger of rarer and more extreme abrupt millennial-scale climate change events.

Section 4: Conclusion

In conclusion, this investigation suggests it is highly likely that explosive volcanism could have triggered millennial-scale climate change over the last 100 ka BP. All modelled $\delta^{18}O$ time-series underpinned by current knowledge of volcanic magnitude-frequency behaviour generated compelling reproductions of the NGRIP $\delta^{18}O$ time-series over the last 100 ka BP, through both graphical comparisons and statistical analysis. This investigation has found that explosive volcanism was especially likely to have triggered both the BA-YD and GS-20 abrupt climate change transitions, as modelled outputs that integrated the known eruption catalogue reproduced these periods well. Furthermore, as the Model 4 ('Combination') time-series output outperformed Model 1 ('Known Eruptions'), this investigation strongly supports the hypothesis that unknown eruptions could have triggered millennial-scale climate change events that occurred during large gaps in the known eruptions catalogue. Future research investigating explosive volcanism as a potential millennial-scale climate trigger should consider eruption dating uncertainties to address offsets between modelled and the NGRIP $\delta^{18}O$ time-series, as well as focussing modelling on shorter windows to investigate the plausibility of explosive volcanism as a potential trigger of millennial-scale climate change at an individual event level.

Finally, the finding that atmospheric CO_2 concentrations modulated climatic baseline conditions and abrupt climate change recovery rates in the statistical model indicates the crucial importance of reducing anthropogenic CO_2 emissions. The exponential relationship between atmospheric CO_2 concentration and millennial-scale climate change GRR (Section 2.1.3) indicates how important low atmospheric CO_2 concentration may be for reducing the

longevity of millennial-scale climate change events, especially after an extremely perturbing large magnitude eruption; reducing atmospheric CO_2 concentration is likely one of the few ways humans can mitigate the severity of abrupt climate change effectively. In the context of modern-day atmospheric CO_2 concentration, the results of this investigation illustrate how crucial it is that climate change forecasts adequately acknowledge the potential severity and abrupt nature of climate change that an explosive eruption could trigger; although modern-day sea-level prevented large millennial-scale climate change events in this investigation, informed forecasting requires further research efforts to gain a better understanding of the potential control of eruption nature and climate boundary conditions on future millennial-scale climate change events.

References

Abbott, P.M., Niemeier, U., Timmreck, C., Riede, F., McConnell, J.R., Severi, M., Fischer, H., Svensson, A., Toohey, M., Reinig, F., Sigl, M., 2021. Volcanic climate forcing preceding the inception of the Younger Dryas: Implications for tracing the Laacher See eruption. *Quaternary Science Reviews* 274, p.107260.

Aiuppa, A., Inguaggiato, S., McGonigle, A.J.S., O'Dwyer, M., Oppenheimer, C., Padgett, M.J., Rouwet, D., Valenza, M., 2005. H2S fluxes from Mt. Etna, Stromboli, and Vulcano (Italy) and implications for the sulfur budget at volcanoes. *Geochimica et Cosmochimica Acta* 69(7) pp. 1861–1871.

Alley, R.B., Clark, P.U., Keigwin, L.D., Webb, R.S., 1999. Making sense of millennial-scale climate change. *Geophysical Monograph-American Geophysical Union* 112, pp. 385–394.

Alley, R.B., Marotzke, J., Nordhaus, W.D., Overpeck, J.T., Peteet, D.M., Pielke, R.A., Pierrehumbert, R.T., Rhines, P.B., Stocker, T.F., Talley, L.D., Wallace, J.M., 2003. Abrupt Climate Change. *Science* 299(5615), pp. 2005–2010.

Andersen, K.K., Azuma, N., Barnola, J.-M., Bigler, M., Biscaye, P., Caillon, N., Chappellaz, J., Clausen, H.B., Dahl-Jensen, D., Fischer, H., Flückiger, J., Fritzsche, D., Fujii, Y., Goto-Azuma, K., Grønvold, K., Gundestrup, N.S., Hansson, M., Huber, C., Hvidberg, C.S., Johnsen, S.J., Jonsell, U., Jouzel, J., Kipfstuhl, S., Landais, A., Leuenberger, M., Lorrain, R., Masson-Delmotte, V., Miller, H., Motoyama, H., Narita, H., Popp, T., Rasmussen, S.O., Raynaud, D., Rothlisberger, R., Ruth, U., Samyn, D., Schwander, J., Shoji, H., Siggard-Andersen, M.-L., Steffensen, J.P., Stocker, T., Sveinbjörnsdóttir, A.E., Svensson, A., Takata, M., Tison, J.-L.,

Thorsteinsson, Th., Watanabe, O., Wilhelms, F., White, J.W.C., members, N.G.I.C.P., 2004. High-resolution record of Northern Hemisphere climate extending into the last interglacial period. *Nature* 431(7005), pp. 147–151.

Armour, K.C., Bitz, C.M., Roe, G.H., 2013. Time-Varying Climate Sensitivity from Regional Feedbacks. *Journal of Climate* 26(13), pp. 4518–4534.

Aubry, T.J., Staunton-Sykes, J., Marshall, L.R., Haywood, J., Abraham, N.L., Schmidt, A., 2021. Climate change modulates the stratospheric volcanic sulfate aerosol lifecycle and radiative forcing from tropical eruptions. *Nature Communications* 12(1), pp. 1–16.

Baldini, J.U.L., Brown, R.J., Mawdsley, N., 2018. Evaluating the link between the sulfur-rich Laacher See volcanic eruption and the Younger Dryas climate anomaly. *Climate of the Past* 14(7), pp. 969–990.

Baldini, J.U.L., Brown, R.J., McElwaine, J.N., 2015. Was millennial scale climate change during the Last Glacial triggered by explosive volcanism? *Scientific Reports* 5(1), p. 17442.

Bard, E., 2002. Climate Shock: Abrupt Changes Over Millennial Time Scales. Physics Today 55(12), pp. 32-38.

Bay, R.C., Bramall, N., Price, P.B., 2004. Bipolar correlation of volcanism with millennial climate change. *Proceedings of the National Academy of Sciences* 101(17), pp. 6341–6345.

Bengston, D.N., Crabtree, J., Hujala, T., 2020. Abrupt climate change: Exploring the implications of a wild card. *Futures* 124, p. 102641.

Bereiter, B., Eggleston, S., Schmitt, J., Nehrbass-Ahles, C., Stocker, T.F., Fischer, H., Kipfstuhl, S., Chappellaz, J., 2015. Revision of the EPICA Dome C CO2 record from 800 to 600-kyr before present. *Geophysical Research Letters* 42(2), pp. 542–549.

Berger, A., 1988. Milankovitch Theory and climate. *Reviews of Geophysics* 26(4), pp. 624–657.

Blunier, T., Brook, E.J., 2001. Timing of Millennial-Scale Climate Change in Antarctica and Greenland during the Last Glacial Period. *Science* 291(5501), pp. 109–112.

Boers, N., 2018. Early-warning signals for Dansgaard-Oeschger events in a high-resolution ice core record. *Nature Communications* 9(1), p. 2556.

Boers, N., Ghil, M., Rousseau, D.-D., 2018. Ocean circulation, ice shelf, and sea ice interactions explain Dansgaard–Oeschger cycles. *Proceedings of the National Academy of Sciences* 115, E11005–E11014.

Bond, G., Broecker, W., Johnsen, S., McManus, J., Labeyrie, L., Jouzel, J., Bonani, G., 1993. Correlations between climate records from North Atlantic sediments and Greenland ice. *Nature* 365(6442), pp. 143–147.

Bowman, J., 1990. The greenhouse effect. *Land Use Policy* 7(2), pp. 101–108.

Braun, H., Kurths, J., 2010. Were Dansgaard-Oeschger events forced by the Sun? *The European Physical Journal Special Topics* 191(1), pp. 117–129.

Brázdil, R., Řezníčková, L., Valášek, H., Dolák, L., Kotyza, O., 2016. Climatic effects and impacts of the 1815 eruption of Mount Tambora in the Czech Lands. *Climate of the Past* 12(6), pp. 1361–1374.

Broecker, W.S., 2006. Was the Younger Dryas triggered by a flood? Science 312, pp. 1146–1148.

Bronk Ramsey, C., Albert, P.G., Blockley, S.P.E., Hardiman, M., Housley, R.A., Lane, C.S., Lee, S., Matthews, I.P., Smith, V.C., Lowe, J.J., 2015. Improved age estimates for key Late Quaternary European tephra horizons in the RESET lattice. *Quaternary Science Reviews* 118, pp. 18–32.

Brönnimann, S., Krämer, D., 2016. *Tambora and the" Year Without a Summer" of 1816. A Perspective on Earth and Human Systems Science* (Vol. 90). Geographica Bernensia.

Brown, S.K., Crosweller, H.S., Sparks, R.S.J., Cottrell, E., Deligne, N.I., Guerrero, N.O., Hobbs, L., Kiyosugi, K., Loughlin, S.C., Siebert, L., Takarada, S., 2014. Characterisation of the Quaternary eruption record: analysis of the Large Magnitude Explosive Volcanic Eruptions (LaMEVE) database. *Journal of Applied Volcanology* 3(5), pp. 1-22.

Bursik, M., 2001. Effect of wind on the rise height of volcanic plumes. *Geophysical Research Letters* 28(18), pp. 3621–3624.

Caillon, N., Severinghaus, J.P., Jouzel, J., Barnola, J.M., Kang, J., Lipenkov, V.Y., 2003. Timing of atmospheric CO2 and antarctic temperature changes across termination III. *Science* 299(5613), pp. 1728–1731.

Campisano, C., 2012. Milankovitch Cycles, Paleoclimatic Change, and Hominin Evolution. *Nature Education Knowledge* 3(5).

Carey, S., Sigurdsson, H., 1989. The intensity of plinian eruptions. *Bulletin of Volcanology* 1989 51(1), pp. 28–40.

Carlson, A.E., 2010. What Caused the Younger Dryas Cold Event? *Geology* 38(4), pp. 383–384.

Cheng, H., Zhang, H., Spötl, C., Baker, J., Sinha, A., Li, H., Bartolomé, M., Moreno, A., Kathayat, G., Zhao, J., Dong, X., Li, Y., Ning, Y., Jia, X., Zong, B., Brahim, Y.A., Pérez-Mejiás, C., Cai, Y., Novello, V.F., Cruz, F.W., Severinghaus, J.P., An, Z., Edwards, R.L., 2020. Timing and structure of the Younger Dryas event and its underlying climate dynamics. *Proceedings of the National Academy of Sciences* 117(38), pp. 23408–23417.

Cimatoribus, A.A., Drijfhout, S.S., Livina, V., van der Schrier, G., 2013. Dansgaard–Oeschger events: bifurcation points in the climate system. *Climate of the Past* 9(1), pp. 323–333.

Cisneros de León, A., Mittal, T., Silva, S.L. de, Self, S., Schmitt, A.K., Kutterolf, S., 2022. On synchronous supereruptions. *Frontiers in Earth Science* 10, pp. 1-10.

Cisneros de León, A., Schindlbeck-Belo, J.C., Kutterolf, S., Danišík, M., Schmitt, A.K., Freundt, A., Pérez, W., Harvey, J.C., Wang, K.L., Lee, H.Y., 2021. A history of violence: magma incubation, timing and tephra distribution of the Los Chocoyos supereruption (Atitlán Caldera, Guatemala). *Journal of Quaternary Science* 36(2), pp. 169–179.

Cline, W.R., 1991. Scientific Basis for the Greenhouse Effect. *The Economic Journal 101*(407), pp. 904-919.

Cole-Dai, J., 2010. Volcanoes and climate. *Wiley Interdisciplinary Reviews: Climate Change* 1(6), pp. 824–839.

Colose, C., LeGrande, A., Vuille, M., 2016. Hemispherically asymmetric volcanic forcing of tropical hydroclimate during the last millennium. *Earth System Dynamics* 7(3), pp. 681-696.

Condron, A., Winsor, P., 2012. Meltwater routing and the Younger Dryas. *Proceedings of the National Academy of Sciences* 109(49), pp. 19928–19933.

Cooper, C.L., Swindles, G.T., Savov, I.P., Schmidt, A., Bacon, K.L., 2018. Evaluating the relationship between climate change and volcanism. *Earth-Science Reviews* 177, pp. 238–247.

Crick, L., Burke, A., Hutchison, W., Kohno, M., Moore, K.A., Savarino, J., Doyle, E.A., Mahony, S., Kipfstuhl, S., Rae, J.W.B., Steele, R.C.J., Sparks, R.S.J., Wolff, E.W., 2021. New insights into the ~74ka Toba eruption from sulfur isotopes of polar ice cores. *Climate of the Past* 17(5), pp. 2119–2137.

Croll, J., Sugden, D., 2021. On the thickness of the Antarctic ice, and its relations to that of the glacial epoch. *Earth and Environmental Science Transactions of the Royal Society of Edinburgh* 112(3-4), pp. 245-252.

Crosweller, H.S., Arora, B., Brown, S.K., Cottrell, E., Deligne, N.I., Guerrero, N.O., Hobbs, L., Kiyosugi, K., Loughlin, S.C., Lowndes, J., Nayembil, M., Siebert, L., Sparks, R.S.J., Takarada, S., Venzke, E., 2012. Global database on large magnitude explosive volcanic eruptions (LaMEVE). *Journal of Applied Volcanology* 1(1), pp. 1–13.

Dansgaard, W., 1985. Greenland ice core studies. *Palaeogeography, Palaeoclimatology, Palaeoecology* 50(2-3), pp. 185–187.

Denton, G.H., Alley, R.B., Comer, G.C., Broecker, W.S., 2005. The role of seasonality in abrupt climate change. *Quaternary Science Reviews* 24(10-11), pp. 1159–1182.

Dima, M., Lohmann, G., Knorr, G., 2018. North Atlantic Versus Global Control on Dansgaard-Oeschger Events. *Geophysical Research Letters* 45(23), pp. 12,991–12,998

Dokken, T.M., Nisancioglu, K.H., Li, C., Battisti, D.S., Kissel, C., 2013. Dansgaard-Oeschger cycles: Interactions between ocean and sea ice intrinsic to the Nordic seas. *Paleoceanography* 28(3), pp. 491–502.

Drexler, J.W., Rose, W.I., Sparks, R.S.J., Ledbetter, M.T., 1980. The Los Chocoyos Ash, Guatemala: A Major Stratigraphic Marker in Middle America and in Three Ocean Basins. *Quaternary Research* 13(3), pp. 327–345.

Durant, A.J., Bonadonna, C., Horwell, C.J., 2010. Atmospheric and Environmental Impacts of Volcanic Particulates. *Elements* 6(4), pp. 235–240.

Fedele, F.G., Giaccio, B., Hajdas, I., 2008. Timescales and cultural process at 40,000 BP in the light of the Campanian Ignimbrite eruption, Western Eurasia. *Journal of Human Evolution* 55, 834–857.

Felzer, B., Webb, T., Oglesby, R.J., 1998. The impact of ice sheets, CO2, and orbital insolation on late quaternary climates: sensitivity experiments with a general circulation model. *Quaternary Science Reviews* 17(6-7), pp. 507–534.

Firestone, R.B., West, A., Kennett, J.P., Becker, L., Bunch, T.E., Revay, Z.S., Schultz, P.H., Belgya, T., Kennett, D.J., Erlandson, J.M., Dickenson, O.J., Goodyear, A.C., Harris, R.S., Howard, G.A., Kloosterman, J.B., Lechler, P., Mayewski, P.A., Montgomery, J., Poreda, R., Darrah, T., Hee, S.S.Q., Smith, A.R., Stich, A., Topping, W., Wittke, J.H., Wolbach, W.S., 2007. Evidence for an extraterrestrial impact 12,900 years ago that contributed to the megafaunal extinctions and the Younger Dryas cooling. *Proceedings of the National Academy of Sciences* 104(41), pp. 16016–16021.

Furlan, C., 2010. Extreme value methods for modelling historical series of large volcanic magnitudes. *Statistical Modelling* 10(2), pp. 113–132.

Ganopolski, A., Rahmstorf, S., 2002. A Theory of Dansgaard-oeschger Events. In *EGS General Assembly Conference Abstracts* (p. 5591).

Genty, D., Blamart, D., Ouahdi, R., Gilmour, M., Baker, A., Jouzel, J., Van-Exter, S., 2003. Precise dating of Dansgaard–Oeschger climate oscillations in western Europe from stalagmite data. *Nature* 421, pp. 833–837.

Gottschalk, J., Skinner, L.C., Misra, S., Waelbroeck, C., Menviel, L., Timmermann, A., 2015. Abrupt changes in the southern extent of North Atlantic Deep Water during Dansgaard–Oeschger events. *Nature Geoscience* 8(12), pp. 950–954.

Gottwald, G.A., 2021. A model for Dansgaard–Oeschger events and millennial-scale abrupt climate change without external forcing. *Climate Dynamics* 56(1), pp. 227–243.

Grant, K.M., Rohling, E.J., Bar-Matthews, M., Ayalon, A., Medina-Elizalde, M., Ramsey, C.B., Satow, C., Roberts, A.P., 2012. Rapid coupling between ice volume and polar temperature over the past 150,000 years. *Nature* 2012 491(7426), pp. 744–747.

Grigg, L.D., Whitlock, C., Dean, W.E., 2001. Evidence for Millennial-Scale Climate Change During Marine Isotope Stages 2 and 3 at Little Lake, Western Oregon, U.S.A. *Quaternary Research* 56(1), pp. 10–22.

Guillevic, M., Bazin, L., Landais, A., Kindler, P., Orsi, A., Masson-Delmotte, V., Blunier, T., Buchardt, S.L., Capron, E., Leuenberger, M., Martinerie, P., Prié, F., Vinther, B.M., 2013. Spatial gradients of temperature, accumulation and δ 18 O-ice in Greenland over a series of Dansgaard–Oeschger events. *Climate of the Past* 9(3), pp. 1029–1051.

Hansen, J., Lacis, A., Ruedy, R., Sato, M., 1992. Potential climate impact of Mount Pinatubo eruption. *Geophysical Research Letters* 19(2), pp. 215–218.

Holliday, V.T., Surovell, T., Meltzer, D.J., Grayson, D.K., Boslough, M., 2014. The Younger Dryas impact hypothesis: a cosmic catastrophe. *Journal of Quaternary Science* 29(6), pp. 515–530.

Hoshyaripour, G., Hort, M., Langmann, B., 2012. How does the hot core of a volcanic plume control the sulfur speciation in volcanic emission? *Geochemistry, Geophysics, Geosystems* 13(7), pp. 1-13.

Humlum, O., Stordahl, K., Solheim, J.E., 2013. The phase relation between atmospheric carbon dioxide and global temperature. *Global and Planetary Change* 100, pp. 51–69.

IPCC, 2021: Summary for Policymakers. In: Climate Change 2021: The Physical Science Basis. Contribution of Working Group I to the Sixth Assessment Report of the Intergovernmental Panel on Climate Change [Masson-Delmotte, V., P. Zhai, A. Pirani, S.L. Connors, C. Péan, S. Berger, N. Caud, Y. Chen, L. Goldfarb, M.I. Gomis, M. Huang, K. Leitzell, E. Lonnoy, J.B.R. Matthews, T.K. Maycock, T. Waterfield, O. Yelekçi, R. Yu, and B. Zhou (eds.)]. Cambridge University Press.

Israde-Alcántara, I., Bischoff, J.L., Domínguez-Vázquez, G., Li, H.-C., DeCarli, P.S., Bunch, T.E., Wittke, J.H., Weaver, J.C., Firestone, R.B., West, A., Kennett, J.P., Mercer, C., Xie, S., Richman, E.K., Kinzie, C.R., Wolbach, W.S., 2012. Evidence from central Mexico supporting the Younger Dryas extraterrestrial impact hypothesis. *Proceedings of the National Academy of Sciences* 109(13), E738–E747.

Kandlbauer, J., Hopcroft, P.O., Valdes, P.J., Sparks, R.S.J., 2013. Climate and carbon cycle response to the 1815 Tambora volcanic eruption. *Journal of Geophysical Research: Atmospheres* 118(22), pp. 12,497-12,507.

Keigwin, L.D., 1999. *Mechanisms of Global Climate Change at Millennial Time Scales*. American Geophysical Union.

Kiyosugi, K., Connor, C., Sparks, R.S.J., Crosweller, H.S., Brown, S.K., Siebert, L., Wang, T., Takarada, S., 2015. How many explosive eruptions are missing from the geologic record? Analysis of the quaternary record of large magnitude explosive eruptions in Japan. *Journal of Applied Volcanology* 4(1), pp. 1–15.

Kukla, G.J., 1972. Insolation and glacials. *Boreas* 1(1), pp. 63–96.

Kuo, C., Lindberg, C., Thomson, D.J., 1990. Coherence established between atmospheric carbon dioxide and global temperature. Nature 343(6260), pp. 709–714.

Kweku, D.W., Bismark, O., Maxwell, A., Desmond, K.A., Danso, K.B., Oti-Mensah, E.A., Quachie, A.T., Adormaa, B.B., 2018. Greenhouse Effect: Greenhouse Gases and Their Impact on Global Warming. *Journal of Scientific Research and Reports* 17(6), pp. 1–9.

Lacis, A.A., Schmidt, G.A., Rind, D., Ruedy, R.A., 2010. Atmospheric CO_2: Principal Control Knob Governing Earth's Temperature. *Science* 330(6002), pp. 356–359.

Lane, C.S., Brauer, A., Martín-Puertas, C., Blockley, S.P.E., Smith, V.C., Tomlinson, E.L., 2015. The Late Quaternary tephrostratigraphy of annually laminated sediments from Meerfelder Maar, Germany. *Quaternary Science Reviews* 122, pp. 192–206.

Lechleitner, F.A., Breitenbach, S.F.M., Rehfeld, K., Ridley, H.E., Asmerom, Y., Prufer, K.M., Marwan, N., Goswami, B., Kennett, D.J., Aquino, V. v., Polyak, V., Haug, G.H., Eglinton, T.I., Baldini, J.U.L., 2017. Tropical rainfall over the last two millennia: evidence for a low-latitude hydrologic seesaw. *Scientific Reports* 7(1), pp. 1–9.

Ledley, T.S., Sundquist, E.T., Schwartz, S.E., Hall, D.K., Fellows, J.D., Killeen, T.L., 1999. Climate change and greenhouse gases. *Eos, Transactions American Geophysical Union* 80(39), pp. 453–458.

Li, C., Born, A., 2019. Coupled atmosphere-ice-ocean dynamics in Dansgaard-Oeschger events. *Quaternary Science Reviews* 203, pp. 1–20.

Ling, Y., Mahadevan, S., 2013. Quantitative model validation techniques: New insights. *Reliability Engineering & System Safety* 111, 217–231.

Lohmann, J., Castellana, D., Ditlevsen, P.D., Dijkstra, H.A., 2021. Abrupt climate change as a rate-dependent cascading tipping point. *Earth System Dynamics* 12(3), pp. 819–835.

Lohmann, J., Ditlevsen, P.D., 2018. Random and externally controlled occurrences of Dansgaard–Oeschger events. *Climate of the Past* 14(5), pp. 609–617.

Lohmann, J., Svensson, A., 2020. On the Role of Volcanism in Dansgaard-Oeschger Cycles. *Climate of the Past Discussions* [preprint], pp. 1–15.

Martis, M.S., 2006. Validation of simulation based models: A theoretical outlook. *Electronic Journal of Business Research Methods* 4(1), pp. 39-46.

McCarroll, D., 2015. 'Study the past, if you would divine the future': a retrospective on measuring and understanding Quaternary climate change. *Journal of Quaternary Science* 30(2), pp. 154–187.

McEwan, B. (2017). Bonferroni correction. In M. Allen (Ed.) *The sage encyclopedia of communication research methods* (pp. 105-106). Available at: https://methods.sagepub.com/reference/the-sage-encyclopedia-of-communication-research-methods/i2264.xml (Accessed: 12 September 2022).

Miller, G.H., Geirsdóttir, Á., Zhong, Y., Larsen, D.J., Otto-Bliesner, B.L., Holland, M.M., Bailey, D.A., Refsnider, K.A., Lehman, S.J., Southon, J.R., Anderson, C., Björnsson, H., Thordarson, T., 2012. Abrupt onset of the Little Ice Age triggered by volcanism and sustained by sea-ice/ocean feedbacks. *Geophysical Research Letters* 39(2).

Minnis, P., Harrison, E.F., Stowe, L.L., Gibson, G.G., Denn, F.M., Doelling, D.R., Smith, W.L., 1993. Radiative Climate Forcing by the Mount Pinatubo Eruption. *Science* 259(5100), pp. 1411–1415.

Moossen, H., Bendle, J., Seki, O., Quillmann, U., Kawamura, K., 2015. North Atlantic Holocene climate evolution recorded by high-resolution terrestrial and marine biomarker records. *Quaternary Science Reviews* 129, pp. 111–127.

Murton, J.B., Bateman, M.D., Dallimore, S.R., Teller, J.T., Yang, Z., 2010. Identification of Younger Dryas outburst flood path from Lake Agassiz to the Arctic Ocean. *Nature* 464(7289), pp. 740–743.

Muschitiello, F., Pausata, F.S.R., Watson, J.E., Smittenberg, R.H., Salih, A.A.M., Brooks, S.J., Whitehouse, N.J., Karlatou-Charalampopoulou, A., Wohlfarth, B., 2015. Fennoscandian freshwater control on Greenland hydroclimate shifts at the onset of the Younger Dryas. *Nature Communications* 6(1), pp. 1–8.

National Research Council (U.S.). Committee on Abrupt Climate Change., 2001. *Abrupt Climate Change : Inevitable Surprises*.

Not, C., Hillaire-Marcel, C., 2012. Enhanced sea-ice export from the Arctic during the Younger Dryas. *Nature Communications* 3(1), pp. 1–5.

Nye, H., Condron, A., 2021. Assessing the statistical uniqueness of the Younger Dryas: A robust multivariate analysis. *Climate of the Past* 17(3), pp. 1409–1421.

Oka, A., Abe-Ouchi, A., Sherriff-Tadano, S., Yokoyama, Y., Kawamura, K., Hasumi, H., 2021. Glacial mode shift of the Atlantic meridional overturning circulation by warming over the Southern Ocean. *Communications Earth & Environment* 2(1), pp. 1–8.

Oppenheimer, C., 2011. *Eruptions that Shook the World*. Cambridge University Press.

Oppenheimer, C., 2002. Limited global change due to the largest known Quaternary eruption, Toba ≈74 kyr BP? *Quaternary Science Reviews* 21(14-15), pp. 1593–1609.

Paine, A.R., Wadsworth, F.B., Baldini, J.U.L., 2021. Supereruption doublet at a climate transition. *Communications Earth & Environment* 2(1), pp. 1–3.

Papale, P., 2018. Global time-size distribution of volcanic eruptions on Earth. *Scientific Reports* 8(1), pp. 1–11.

Pasini, A., Triacca, U., Attanasio, A., 2012. Evidence of recent causal decoupling between solar radiation and global temperature. *Environmental Research Letters* 7(3), p. 034020.

Pausata, F.S.R., Chafik, L., Caballero, R., Battisti, D.S., 2015. Impacts of high-latitude volcanic eruptions on ENSO and AMOC. *Proceedings of the National Academy of Sciences* 112(45), pp. 13784–13788.

Pausata, F.S.R., Zanchettin, D., Karamperidou, C., Caballero, R., Battisti, D.S., Battisti, D.S., 2020. ITCZ shift and extratropical teleconnections drive ENSO response to volcanic eruptions. *Science Advances* 6(23), pp.1-11.

Petersen, S. v, Schrag, D.P., Clark, P.U., 2013. A new mechanism for Dansgaard-Oeschger cycles. *Paleoceanography* 28(1), pp. 24-30.

Polyak, V.J., Asmerom, Y., Lachniet, M.S., 2017. Rapid speleothem δ13C change in southwestern North America coincident with Greenland stadial 20 and the Toba (Indonesia) supereruption. *Geology* 45(9), pp. 843–846.

Proctor, J., Hsiang, S., Burney, J., Burke, M., Schlenker, W., 2018. Estimating global agricultural effects of geoengineering using volcanic eruptions. Nature 560(7719), pp. 480–483.

Ramaswamy, V., Ramachandran, S., Stenchikov, G., Robock, A., 2006. A model study of the effect of Pinatubo volcanic aerosols on stratospheric temperatures. *Frontiers of Climate Modeling* (9780521791328), pp. 152–178.

Rasmussen, S.O., Bigler, M., Blockley, S.P., Blunier, T., Buchardt, S.L., Clausen, H.B., Cvijanovic, I., Dahl-Jensen, D., Johnsen, S.J., Fischer, H., Gkinis, V., Guillevic, M., Hoek, W.Z., Lowe, J.J., Pedro, J.B., Popp, T., Seierstad, I.K., Steffensen, J.P., Svensson, A.M., Vallelonga, P., Vinther, B.M., Walker, M.J.C., Wheatley, J.J., Winstrup, M., 2014. A stratigraphic framework for abrupt climatic changes during the Last Glacial period based on three synchronized Greenland ice-core records: refining and extending the INTIMATE event stratigraphy. *Quaternary Science Reviews* 106, pp. 14–28.

Reinig, F., Wacker, L., Jöris, O., Oppenheimer, C., Guidobaldi, G., Nievergelt, D., Adolphi, F., Cherubini, P., Engels, S., Esper, J., Land, A., Lane, C., Pfanz, H., Remmele, S., Sigl, M., Sookdeo, A., Büntgen, U., 2021. Precise date for the Laacher See eruption synchronizes the Younger Dryas. *Nature* 595(7865), pp. 66–69.

Ridley, H.E., Asmerom, Y., Baldini, J.U.L., Breitenbach, S.F.M., Aquino, V. v., Prufer, K.M., Culleton, B.J., Polyak, V., Lechleitner, F.A., Kennett, D.J., Zhang, M., Marwan, N., Macpherson, C.G., Baldini, L.M., Xiao, T., Peterkin, J.L., Awe, J., Haug, G.H., 2015. Aerosol forcing of the position of the intertropical convergence zone since ad 1550. *Nature Geoscience* 8(3), pp. 195–200.

Ridley, J., Gregory, J.M., Huybrechts, P., Lowe, J., 2010. Thresholds for irreversible decline of the Greenland ice sheet. *Climate Dynamics* 35(6), pp. 1065–1073.

Riechers, K., Boers, N., 2021. Significance of uncertain phasing between the onsets of stadial–interstadial transitions in different Greenland ice core proxies. *Climate of the Past* 17(4), pp. 1751–1775.

Robock, A., 2000. Volcanic eruptions and climate. *Reviews of Geophysics* 38(2), pp. 191–219.

Robock, A., Ammann, C.M., Oman, L., Shindell, D., Levis, S., Stenchikov, G., 2009. Did the Toba volcanic eruption of ~74 ka B.P. produce widespread glaciation? *Journal of Geophysical Research: Atmospheres* 114(D10107), pp. 1-9.

Rohling, E.J., Braun, K., Grant, K., Kucera, M., Roberts, A.P., Siddall, M., Trommer, G., 2010. Comparison between Holocene and Marine Isotope Stage-11 sea-level histories. *Earth and Planetary Science Letters* 291(1-4), pp. 97–105.

Rougier, J., Sparks, R.S.J., Cashman, K. v., Brown, S.K., 2018. The global magnitude–frequency relationship for large explosive volcanic eruptions. *Earth and Planetary Science Letters* 482, pp. 621–629.

Rozanski, K., Araguãs-Araguãs, L., Gonfiantini, R., 1992. Relation Between Long-Term Trends of Oxygen-18 Isotope Composition of Precipitation and Climate. *Science* 258(5084), pp. 981–985.

Ruddiman, W.F., Fuller, D.Q., Kutzbach, J.E., Tzedakis, P.C., Kaplan, J.O., Ellis, E.C., Vavrus, S.J., Roberts, C.N., Fyfe, R., He, F., Lemmen, C., Woodbridge, J., 2016. Late Holocene climate: Natural or anthropogenic? *Reviews of Geophysics* 54(1), pp. 93–118.

Scaillet, B., Clemente, B., Evans, B.W., Pichavant, M., 1998. Redox control of sulfur degassing in silicic magmas. *Journal of Geophysical Research: Solid Earth* 103(B10), pp. 23937–23949.

Schalter, N., Griesser, T., Fischer, A.M., Sticker, A., Brönnimann, S., 2009. Climate effects of the 1883 Krakatoa eruption. *Vierteljahrsschrift der Naturforschenden Gesellschaft in Zürich* 154(1/2), pp. 31–40.

Schulz, M., 2002. On the 1470-year pacing of Dansgaard-Oeschger warm events. *Paleoceanography* 17(2), pp. 4–9.

Self, S., 2006. The effects and consequences of very large explosive volcanic eruptions. *Philosophical Transactions of the Royal Society A: Mathematical, Physical and Engineering Sciences* 364(1845), pp. 2073–2097.

Shakun, J.D., Clark, P.U., He, F., Marcott, S.A., Mix, A.C., Liu, Z., Otto-Bliesner, B., Schmittner, A., Bard, E., 2012. Global warming preceded by increasing carbon dioxide concentrations during the last deglaciation. *Nature* 484(7392), pp. 49–54.

Sigurdsson, H., 1990. Assessment of the atmospheric impact of volcanic eruptions, in: *Global Catastrophes in Earth History* (247), pp. 99-110. Geological Society of America.

Spratt, R.M., Lisiecki, L.E., 2016. A Late Pleistocene sea level stack. *Climate of the Past* 12(4), pp. 1079–1092.

Stenchikov, G.L., Kirchner, I., Robock, A., Graf, H.-F., Antuña, J.C., Grainger, R.G., Lambert, A., Thomason, L., 1998. Radiative forcing from the 1991 Mount Pinatubo volcanic eruption. *Journal of Geophysical Research: Atmospheres* 103(D12), pp. 13837–13857.

Stenni, B., Buiron, D., Frezzotti, M., Albani, S., Barbante, C., Bard, E., Barnola, J.M., Baroni, M., Baumgartner, M., Bonazza, M., Capron, E., Castellano, E., Chappellaz, J., Delmonte, B., Falourd, S., Genoni, L., Iacumin, P., Jouzel, J., Kipfstuhl, S., Landais, A., Lemieux-Dudon, B., Maggi, V., Masson-Delmotte, V., Mazzola, C., Minster, B., Montagnat, M., Mulvaney, R., Narcisi, B., Oerter, H., Parrenin, F., Petit, J.R., Ritz, C., Scarchilli, C., Schilt, A., Schüpbach, S., Schwander, J., Selmo, E., Severi, M., Stocker, T.F., Udisti, R., 2011. Expression of the bipolar see-saw in Antarctic climate records during the last deglaciation. *Nature Geoscience* 4(1), pp. 46–49.

Stocker, T.F., Johnsen, S.J., 2003. A minimum thermodynamic model for the bipolar seesaw. *Paleoceanography* 18(4), pp. 1-11.

Storey, M., Roberts, R.G., Saidin, M., 2012. Astronomically calibrated 40Ar/39Ar age for the Toba supereruption and global synchronization of late Quaternary records. *Proceedings of the National Academy of Sciences* 109(46), pp. 18684–18688.

Sun, N., Brandon, A.D., Forman, S.L., Waters, M.R., Befus, K.S., 2020. Volcanic origin for Younger Dryas geochemical anomalies ca. 12,900 cal B.P. *Science Advances* 6(31), p.eaax8587.

Swingedouw, D., Mignot, J., Ortega, P., Khodri, M., Menegoz, M., Cassou, C., Hanquiez, V., 2017. Impact of explosive volcanic eruptions on the main climate variability modes. *Global and Planetary Change* 150, pp. 24–45.

Timmreck, C, 2012. Modelling the climatic effects of large explosive volcanic eruptions. *Wiley Interdisciplinary Reviews: Climate Change* 3(6), pp. 545–564.

Toohey, M., Krüger, K., Sigl, M., Stordal, F., Svensen, H., 2016. Climatic and societal impacts of a volcanic double event at the dawn of the Middle Ages. *Climatic Change* 136(3), pp. 401–412.

Wallmann, K., 2014. Is late Quaternary climate change governed by self-sustained oscillations in atmospheric CO2? *Geochimica et Cosmochimica Acta* 132, pp. 413–439.

Williams, M.A.J., Ambrose, S.H., van der Kaars, S., Ruehlemann, C., Chattopadhyaya, U., Pal, J., Chauhan, P.R., 2009. Environmental impact of the 73 ka Toba super-eruption in South Asia. *Palaeogeography, Palaeoclimatology, Palaeoecology* 284(3-4), pp. 295–314.

Wilson, L., Sparks, R.S.J., Huang, T.C., Watkins, N.D., 1978. The control of volcanic column heights by eruption energetics and dynamics. *Journal of Geophysical Research: Solid Earth* 83(B4), pp. 1829–1836.

Zhang, X., Knorr, G., Lohmann, G., Barker, S., 2017. Abrupt North Atlantic circulation changes in response to gradual CO2 forcing in a glacial climate state. *Nature Geoscience* 10(7), pp. 518–523.

Zhang, X., Lohmann, G., Knorr, G., Purcell, C., 2014. Abrupt glacial climate shifts controlled by ice sheet changes. *Nature* 512(7514), pp. 290–294.

Zielinski, G.A., Mayewski, P.A., Meeker, L.D., Whitlow, S., Twickler, M.S., Taylor, K., 1996. Potential atmospheric impact of the Toba mega-eruption ~71,000 years ago. *Geophysical Research Letters* 23(8), pp. 837–840.

Appendix

Appendix 1

Details of all known eruptions used to trigger abrupt climate change events in Model 1 ('Known Eruptions') and Model 4 ('Combination'). Negative magnitudes represent NH eruptions; positive magnitudes represent SH eruptions.

Volcano	Year of Eruption (a BP)	Magnitude *(M)*
Long Island	304	6.3
Huaynaputina	350	6.1
Healy	590	5.9
Okataina	640	6.3
Rinjani	693	6.4
Cotopaxi	719	5.1
Billy Mitchell	849	5.8
Dakataua	998	7.4
Changbaishan	1008	-7.4
Churchill	1103	-6.1
Pago	1106	6.3
Pago	1260	5.8
Rabaul	1267	6
Maca	1400	5.2
Krakatau	1534	7.1
Pago	1640	5.8

Volcano	Year of Eruption (a BP)	Magnitude *(M)*
Ksudach	1710	-6.2
Taupo	1720	6.9
Ambrym	1760	6.8
Churchill	1837	-6.2
Okmok	2026	-6.7
Misti, El	2030	5.2
Antillanca Group	2180	5.5
Atacazo	2232	5.3
Sollipulli	2927	5.9
Aguilera	3200	5.8
Pago	3320	6.5
Taupo	3410	6.2
Vesuvius	3500	-6.6
Santorini	3560	-6.5
Aniakchak	3595	-6.9
Villarrica	3800	5.7
Burney, Monte	4270	5.4
Long Island	4353	6.3
Cotopaxi	4808	5.4
Atacazo	5040	5.2
Pinatubo	5500	-6.1

Volcano	Year of Eruption (a BP)	Magnitude *(M)*
Okataina	5530	6
Fisher	5841	-6.2
Pago	5950	6
Cotopaxi	6574	5.8
Macauley Island	7170	6.7
Mashu	7500	-6.3
Mentolat	7530	5.1
Crater Lake	7627	-6.8
Khangar	7649	-6.3
Hudson, Cerro	7710	6.3
Okataina	8010	5.8
Karkar	8268	6
Tao-Rusyr Caldera	8290	-7
Kurile Lake	8387	-7.2
Cotopaxi	8487	5.8
Vesuvius	8890	-6.1
Burney, Monte	9400	5.5
Okataina	9510	5.7
Chaitén	9700	5.5
Taupo	10080	5.5
Grímsvötn	10180	-6.6

Volcano	Year of Eruption (a BP)	Magnitude *(M)*
Minchinmávida	10380	6
Lvinaya Past	10650	-7
Longonot	10860	6.7
Taupo	11190	5.4
Toluca, Nevado de	12450	-6.3
Laacher See	12880	-6.2
Okataina	13598	6.4
Mashu	13850	-6.2
Reclus	14817	6
Misti, El	14984	5.2
Okataina	15425	5.4
Hudson, Cerro	17370	6.3
Okataina	17625	6.1
Agua de Pau	17838	-6.1
Rabaul	20982	6
Okataina	21800	5.9
Taranaki [Egmont]	23649	5.3
Sete Cidades	24691	-6.1
Okataina	25271	6.5
Kerguelen Islands	26000	6.7
Diablotins, Morne	26581	-6.1

Volcano	Year of Eruption (a BP)	Magnitude *(M)*
Taupo	27100	8.1
Nemo Peak	28084	-6.7
Apoyo	28762	-6.2
Misti, El	29796	5.4
Láscar	30000	6.3
Taupo	30092	5.8
Sheveluch	32161	-6.2
Okataina	32301	6
Menengai	33000	6.4
Trois Pitons, Morne	36385	-6.4
Misti, El	36585	5.4
Rabaul	38640	5.7
Misti, El	38716	5.4
Erebus	39000	6
Misti, El	39174	5.2
Campi Flegrei	39300	-7.1
Krasheninnikov	42410	-6.4
Chillán, Nevados de	42565	6
Ksudach	43858	-6.8
Pacaya	44716	-6.6
Opala	44902	-7

Volcano	Year of Eruption (a BP)	Magnitude *(M)*
Coatepeque Caldera	56900	-6.3
Ischia	58000	-7.1
Kapenga	61000	6.4
Akademia Nauk	69400	-6.1
Coatepeque Caldera	70000	-6.6
Toba	73880	-8.8
Atitlán	75000	-8.1
Asosan	87000	-7.7
Rabaul	100000	6

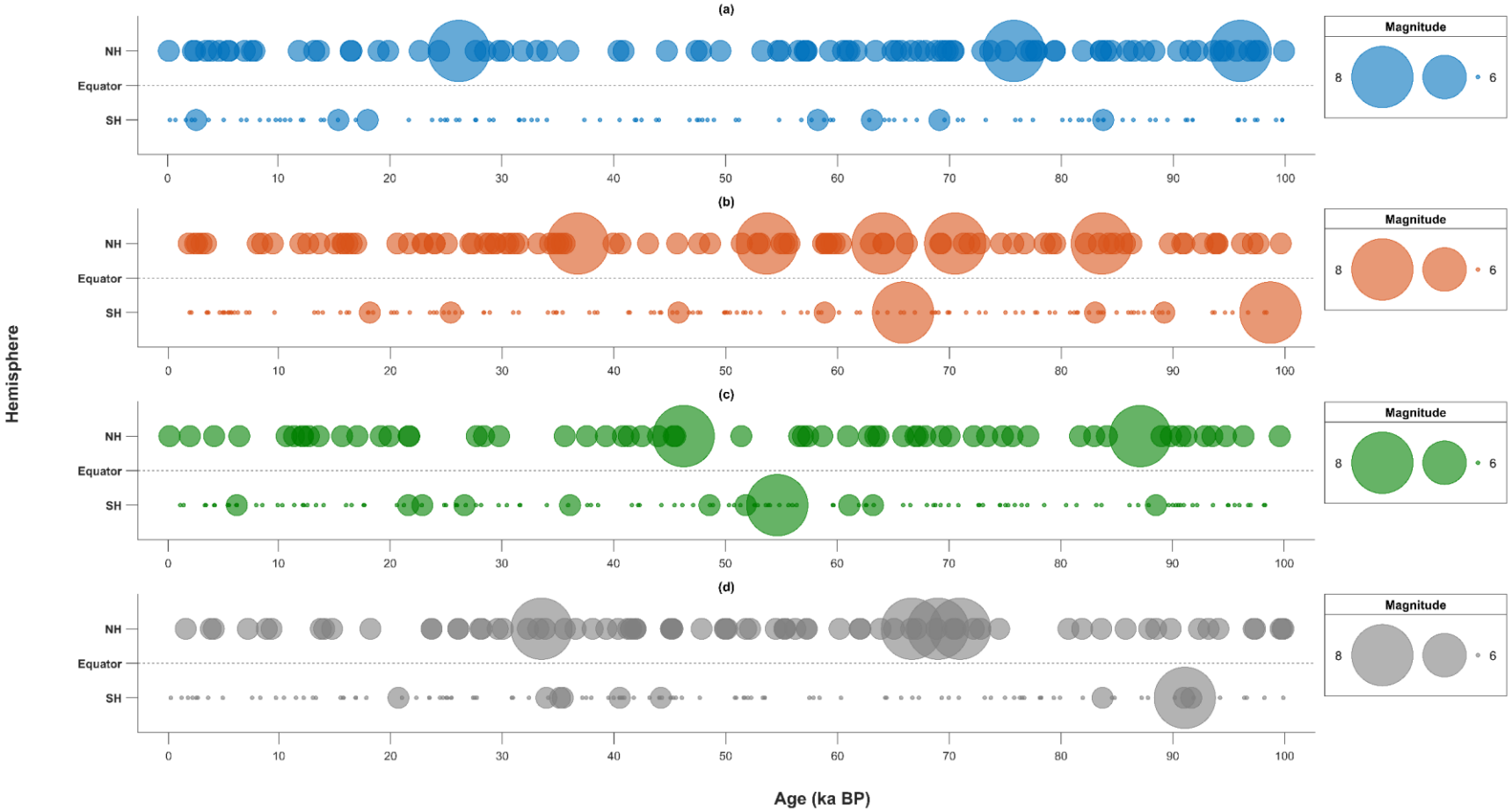

Appendix 2: Examples of volcanic eruption time-series generated by Model 3 ('Weighted Probability'). Time-series used include the 'best' Model 3 generated volcanic eruption time-series (a) and three random time-series (b,c,d). This figure illustrates the high degree of variation produced by each iteration of the model, justifying the use of a Monte Carlo simulation approach to ensure thorough testing of each model.